From the Department of Neuroscience
Karolinska Institutet, Stockholm, Sweden

PRINCIPLES OF REGIONAL COVARIANCE IN BRAIN STRUCTURE

Lars Forsberg

Karolinska Institutet

Stockholm 2022

All previously published papers were reproduced with permission from the publisher.
Talairach atlas figure was reproduced with permission from Thieme.
Published by Karolinska Institutet.
Printed by Universitetsservice US-AB, 2022.

ISBN 978-91-8016-711-6

Cover illustration: A standard brain and regional atlas of 314 older individuals, average age 75 years, from the Ages Gene/Environment Susceptibility (AGES) - Reykjavik Study.

PRINCIPLES OF REGIONAL COVARIANCE IN BRAIN STRUCTURE

THESIS FOR DOCTORAL DEGREE (Ph.D.)

By

Lars Forsberg

The thesis will be defended in public at Samuelssonsalen, Tomtebodavägen 6, Karolinska Institutet, Solna, on the 22nd of September 2022, at 1 pm.

Principal supervisor:
Professor Fredrik Ullén
Karolinska Institutet
Department of Neuroscience

Co-supervisor:
Professor Vilmundur Guðnason
The University of Iceland

Opponent:
Professor Andrea Mechelli
King's College London
Department of Psychosis Studies

Examination board:
Professor Peter Fransson
Karolinska Institutet
Department of Clinical Neuroscience

Professor Hedvig Kjellström
Royal Institute of Technology
Division of Robotics, Perception and Learning

Professor Gilad Silberberg
Karolinska Institutet
Department of Neuroscience

To my family

Abstract

The human brain varies between individuals in both shape and size. These variations are not unique for each brain region. This causes grey matter density between regions to covary, a phenomenon known as "structural brain covariance". The reasons for this structural covariance, and its possible relations to functional connectivity, remain poorly understood. In order to study this morphological variation, a standard brain atlas – also called a brain template – is commonly used to enable consolidation of information across individuals. In the early days of computerised brain research, this was done by creating an average of a large number of brain images from young adults resampled into a common stereotaxic space known as the "MNI space", which is still widely used today. However, this space is less ideal for ageing studies since the brain changes structurally with age.

The aim of this thesis was to provide a deeper understanding of the principles governing structural covariance across the age span. In **Study I**, the need of a computerised brain atlas in ageing was addressed by constructing a standard non-linear brain template from 314 older individuals (average age 75 years) together with a regional atlas and corresponding tissue probability maps. This template was constructed to be linearly mapped to MNI space while forming its own non-linear ageing space. The tissue probability maps also allowed us to construct a non-linear transformation to other spaces and warp the regional atlas to other study cohorts. This approach was used in **Study II-IV**.

In **Study II**, the nature of structural covariance in ageing was investigated by calculating for each grey matter voxel (data point) its number of significant correlations with all the other grey matter voxels in the brain, in a large sample of 960 healthy individuals (age range 68-83 years). Voxels with many significant correlations (known as "hubs") were found in the basal ganglia, the thalamus, the brainstem, and the cerebellum. No significant difference in the covariance structure could be found between relatively younger (68-75 years) and older (76-83 years) individuals or between men and women, suggesting that the hubs represent a fundamental property of structural brain variation that is relatively unaffected by the ageing process.

Study III investigated if the subcortical hub regions from Study II would also be present as hubs with a high level of covariation in a study cohort of 138 young adults between 18-35 years. Secondly, we explored if the observed patterns of structural covariation were related to patterns of functional connectivity during resting state. We replicated the finding from **Study II** that the basal ganglia, the thalamus, and the brainstem were structural hub regions, further strengthening the support that these hubs are not caused by old age. Comparisons of structural covariance patterns and patterns of functional connectivity during rest demonstrated only limited overlap, suggesting that functional connectivity does not cause structural covariance as a general principle.

In the final study (**Study IV**), a dimensionality reduced latent space representation of the cohort from Study III was examined using a convolutional variational autoencoder. The results revealed that only four dimensions – or latent factors – were required to reconstruct most of the structural covariance, including the hubs. Regions with low overall structural covariability typically showed an inconsistent pattern of intercorrelations with other regions in their scores on different factors (e.g. significantly correlated on one factor, but not on other factors). In contrast, hub regions tended to covary across the whole latent space. The factors that correlated positively with the subcortical hubs were also positively related to an increase in functional connectivity during resting state in wide-spread cortical regions.

In summary, these results show that subcortical hubs in human brains are robust across the age span and that structural covariance only shows weak relations to patterns of functional connectivity. Further studies in genetically informative samples would be required to investigate the genetic basis of structural covariation in the human brain.

List of publications and manuscripts

This doctorial thesis is based on the following articles, which are referred to in the text by their Roman numerals and are reproduced in full at the end of the thesis.

I. **Lars Forsberg**, Sigurdur Sigurdsson, Jesper Fredriksson, Asdis Egilsdottir, Bryndis Oskarsdottir, Olafur Kjartansson, Mark A. van Buchem, Lenore J. Launer, Vilmundur Gudnason, and Alex Zijdenbos, 2017. **The AGES-Reykjavik study atlases: Non-linear multi-spectral template and atlases for studies of the ageing brain.** *Medical Image Analysis 39: 133–144.*

II. **Lars Forsberg**, Sigurdur Sigurdsson, Lenore J. Launer, Vilmundur Gudnason, and Fredrik Ullén, 2019. **Structural covariability hubs in old age.** *NeuroImage 189: 307–315.*

III. **Lars Forsberg**, Örjan de Manzano, Vilmundur Gudnason, and Fredrik Ullén, 2022. **Structural covariance and functional connectivity in the human brain.** *Manuscript.*

IV. **Lars Forsberg**, Örjan de Manzano, Vilmundur Gudnason, and Fredrik Ullén, 2022. **Latent space representation of structural covariance in the human brain.** *Manuscript.*

List of publications not included in this thesis

- Per Roland, Gert Svensson, Tony Lindeberg, Tore Risch, Peter Baumann, Andreas Dehmel, Jesper fredriksson, Hjörleifur Halldorson, **Lars Forsberg**, Jeremy Young, and Karl Zilles, 2001. **A database generator for human brain imaging.** *Trends Neurosci 24 (10): 562–564*

- Jeremy P Young and **Lars E Forsberg**, 2005. **Simulating activations with cytoarchitecture.** *Anat. Embryol. 210: 407–410*

- Anna Grabowska, Malgorzata Gut, Andrzej Urbanik, **Lars E Forsberg**, Marek Binder, Barara Sobiecka, and Justyna Kobuz, 2006. **Motor control in left-handed subjects. A functional MR imaging study.** *International Journal of Psychophysiology 61*

- Malgorzata Gut, Andrzej Urbanik, **Lars Forsberg**, Marek Binder, and Krystyna Rymarczyk, 2007. **Brain correlates of right-handedness.** *Acta Neurobiologiae Experimentalis 67: 43–51*

- Anna Grabowska, Malgorzata Gut, Marek Binder, **Lars Forsberg**, and Krystyna Ryarczyk, 2012. **Switching handedness: fMRI study of hand motor control in right-handers, left-handers and converted left-handers.** *Acta Neurobiologiae Experimentalis 72: 439–451*

- Sigurdur Sigurdsson, Thor Aspelund, **Lars Forsberg**, Jesper Fredriksson, Olafuf Kjartansson, Bryndis Oskarsdottir, Palmi V Jonsson, Gudny Eiriksdottir, Tamara B Harris, Alex Zijdenbos, Mark A van Buchem, Lenore Launer, and Vilmundur Gudnason, 2012. **Brain tissue volumes in the general population of the elderly. the AGES-Reykjavik study.** *Neuroimage 59: 3852–3870*

- Laura W de Jong, **Lars E Forsberg**, Jean-Sébastien Vidal, Sigurdur Sigurdsson, Alex P Zijdenbos, Melissa Garcia, Gudny Eiriksdottir, Vilmundur Gudnason, Mark A van Buchem, and Lenore Launer, 2014. **Different susceptibility of medial temporal lobe and basal ganglia atrophy rates to vascular risk factors.** *Neurobiology of aging 35: 72–78*

- Sigurdur Sigurdsson, **Lars Forsberg**, Thor Aspelund, Rob J van der Geest, Mark A van Buchem, Lenore Launer, Vilmundur Gudnason, and Matthias J van Osch, 2015. **Feasibility of Using Pseudo-Continuous Arterial Spin Labeling Perfusion in a Geriatric Population at 1.5 Tesla.** *PLoS ONE 10*

- **Lars E Forsberg**, Lars H Bonde, Michael A Harvey, and Per E Roland, 2016. **The Second Spiking Threshold: Dynamics of Laminar Network Spiking in the Visual Cortex.** *Frontiers in Systems Neuroscience 10, 65*

- Laura W de Jong, Jean-Sébastien Vidal, **Lars E Forsberg**, Alex P Zijdenbos, Thaddeus Haight, Alzheimer's Disease Neuroimaging Initiative, Sigurdur Sigurdsson, Vilmundur Gudnason, Mark A van Buchem, and Lenore J Launer, 2017. **Allometric Scaling of Brain Regions to Intra-Cranial Volume: An Epidemiological MRI Study.** *Human Brain Mapping 38: 151–164*

- Per E Roland, Lars H Bonde, **Lars E Forsberg**, and Michael A Harvey, 2017. **Breaking the Excitation-Inhibition Balance Makes the Cortical Network's Space-Time Dynamics Distingiush Simple Visual Scenes.** *Frontiers in Systems Neuroscience 11, 14*

Contents

List of abbreviations

AAL	Automated Anatomical Labelling
AC	Anterior Commissure
AGES	Age Gene/Environmental Susceptibility
AP	Anterior Point
BOLD	Blood Oxygen Level Dependent
CBA	Computerized Brain Atlas
CSF	Cerebrospinal Fluid
CV	Coefficient of Variation
DSC	Dice Similarity Coefficient
fGBC	Functional Global Brain Connectivity
FIQ	Full Scale IQ
fMRI	Functional Magnetic Resonance Imaging
GLM	General Linear Model
GM	Grey Matter
HBA	Human Brain Atlas
ICA	Independent Component Analysis
ICBM	International Consortium for Brain Mapping
IoI	Index of Individuality
IP	Inferior Point
LP	Left Point
MNI	Montreal Neurological Institute
MR	Magnetic Resonance
MRI	Magnetic Resonance Imaging
NWM	Normal White Matter
PC	Posterior Commissure
PCA	Principal Component Analysis
PET	Positron Emission Tomography
PICA	Probabilistic Independent Component Analysis
PP	Posterior Point
rCBF	Regional Cerebral Blood Flow
RP	Right Point
SP	Superior Point
VAC	Vertical AC line
VBM	Voxel-Based Morphometry
VPC	Vertical PC line
WM	White Matter
WMH	White Matter Hyperintensities

1 Introduction

1.1 Background

Brains are remarkably similar, even between species. For instance, many properties of the basal ganglia, such as its overall organisation and connections to other regions in the brain, are indeed close to identical between all vertebrates. That may be explained by the fact that the basal ganglia constitute a core circuitry in the brain, involved in the selection of behaviour and motor learning, that evolved over 560 million years ago (Grillner and Robertson, 2016).

Brains are obviously also very different between species. This diversity does not merely reflect the fact that larger and more cognitive advanced animals have larger brains. Consider for instance the dolphin brain, which resembles the human brain in both size and complexity, but has a larger cerebellum where the cerebellar lobules are specialised in echolocation (Hanson et al., 2013). In fact, all cetaceans (dolphins, porpoises, and great whales) have developed specific brain features adapted for their marine environment not seen and not needed by mammals living on land (Morgane et al., 1990).

Behavioural differences matter too. Carnivores that have a larger home range tend to also have a larger cerebellum (Chambers et al., 2021). There are also associations between diet, foraging strategy, habitat, and relative brain size between mammals (Mace et al., 1981). This diversity leads to differences in brain structure while maintaining fundamental similarities (Kaiser and Varier, 2011). In general, inter-species differences in brain structure seem therefore to be related to evolutionary processes governed by natural selection to better fit different environments.

Even brains within the same species, such as the human brain, differ in both shape and size between individuals. Ageing is one of the factors that has a great impact on human brain volume, with reductions in both grey matter (GM) and white matter (WM) (Sigurdsson et al., 2012). Genetic variation is another factor that has shown to covary with regional brain volume (Bryant et al., 2013; Zhao et al., 2019). However, even when genetic and ageing variations are controlled for, there will still be a brain variance due to environmental differences (Manzano and Ullén, 2018).

This raises an important question. What are the fundamental principles that govern these differences in human brain morphology? The aim of this thesis is to investigate these principles of structural brain organisation at old age and in young adulthood using large scale computational methods.

1.2 Brain atlases

1.2.1 Brodmann atlas

Sir William Macewen was a pioneer in brain surgery who lived during the 19th century. His methods were for the time rather astonishing as he was able to successfully perform the first removal of a lesion (meningioma) in 1879 (Macmillan, 2005). It was especially astonishing given the fact that he did not have any sort of brain atlas for guidance, but had to rely entirely on observed focal epileptic signs. Illustrations did exist of course and much of the understanding regarding the brain was made by anatomists such as Friedrich Tiedemann (who studied the brain of the fetus and the brain structure in animals) (Idelberger, 1936), Paul Broca (who discovered the speech production center) (LaPointe, 2014), and Carl Wernicke (who discovered the area for speech comprehension) (Pillmann, 2003).

However, it was also in the 19th century that scientists began to work on studying the cytoarchitectural structure of the brain, starting with psychiatrist Theodor Meynert who studied regional differences based on cellular structure in the year 1867 (Triarhou, 2021). Other scientists followed and in 1909 the very first comprehensive brain atlas was published by Korbinian Brodmann, with the definition of 52 areas in the cerebral cortex based on cytoarchitecture (see Figure 1.1) (Brodmann, 1909). This atlas of the brain was so unique and comprehensive that it still influences an entire brain imaging field today (Strotzer, 2009; Zilles, 2018).

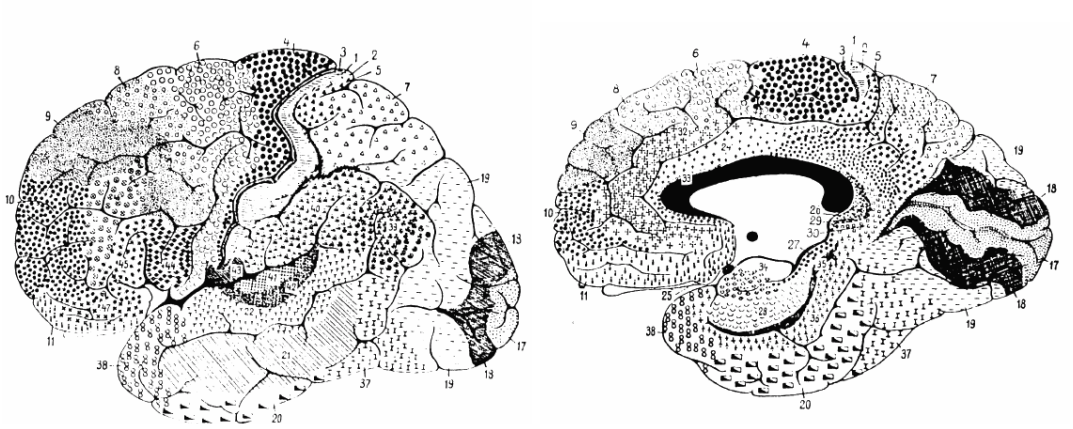

Figure 1.1: The Brodmann atlas.

1.2.2 Talairach atlas

One would think that the Brodmann atlas would improve surgery of the brain, which during the early 20th century was imprecise and difficult. However, because the human brain varies in shape and size, it was very difficult to localise specific GM nuclei in an individual's brain. In 1947, Jean Talairach therefore designed a surgical frame with support for various sizes of the human brain, which was used for grey nuclei localisation in brain surgery. This new method had a profound influence on brain surgery, as it allowed for increased accuracy in the localisation of deep grey nuclei. Later, in 1952, Talairach further improved his stereotaxic system by using the anterior and posterior commissures as reference points for a brain coordinate system. This work was released as a brain atlas of GM nuclei in 1957, followed by a stereotaxic atlas in 1967 of the cerebrum to be used for the surgery of epilepsy (Mazoyer, 2008). The 1967 version of the atlas also contained labels of the Brodmann areas, based on Brodmann's atlas from 1909 (see example in Friedman et al. (1998)). Eventually, this was further developed into an atlas for guidance of deep brain surgery that was released in 1988 (see Figure 1.2) (Talairach and Tournoux, 1988).

The earliest use of the Talairach atlas to approximate locations in functional brain mapping is possibly from a study of stereognostic testing back in 1976 by Roland with colleagues using a gamma camera technique to measure changes in regional cerebral blood flow (rCBF) (Roland and Larsen, 1976). In 1980, this technique was further improved to study changes of rCBF in the supplementary motor area at a group level by transferring the individual results to a brain of standard dimensions similar to the Talairach atlas and then averaging the results across individuals (Roland et al., 1980). A few years later, in 1985, Fox with colleagues developed a similar method for anatomical localisation of functional activation in positron emission tomography (PET) using the Talairach atlas as a stereotactic framework; this time in a fully 3D stereotaxic space (Fox et al., 1985).

When finally the 1988 version of the Talairach atlas came, computerised functional human brain mapping was getting more advanced. Although the main purpose of the atlas was still to facilitate brain surgery, it nevertheless had a large impact on the entire brain mapping field as it allowed consolidating information across individuals with various brain size to an even larger degree than before.

The widespread use of a standardised 3D coordinate system allowed the scientists to report their findings from brain mapping experiments in a common space, which was to be called the "Talairach space". This procedure involved manually identifying a line between the anterior and posterior commissures (AC-PC line) and the location of six other landmarks in each brain (the anterior point (AP), the posterior point (PP), the superior point (SP), the inferior point (IP), the right point (RP), and the left point (LP)), then applying piecewise linear mapping between these points to transform the coordinates of a single brain to the Talairach space (see Figure 1.3).

1.2.3 Computerised brain templates

It was a tedious process to manually identify different landmarks in each PET image and use these to transform the 3D foci of functional activity to Talairach space. One issue was that PET images lacked details on anatomical structure and it was therefore challenging to correctly identify all landmarks. Evans et al. (1992) therefore proposed a method in which a T1-weighted Magnetic Resonance image (MR image, or MRI) of the subject's brain could be used for the labelling of the different landmarks.

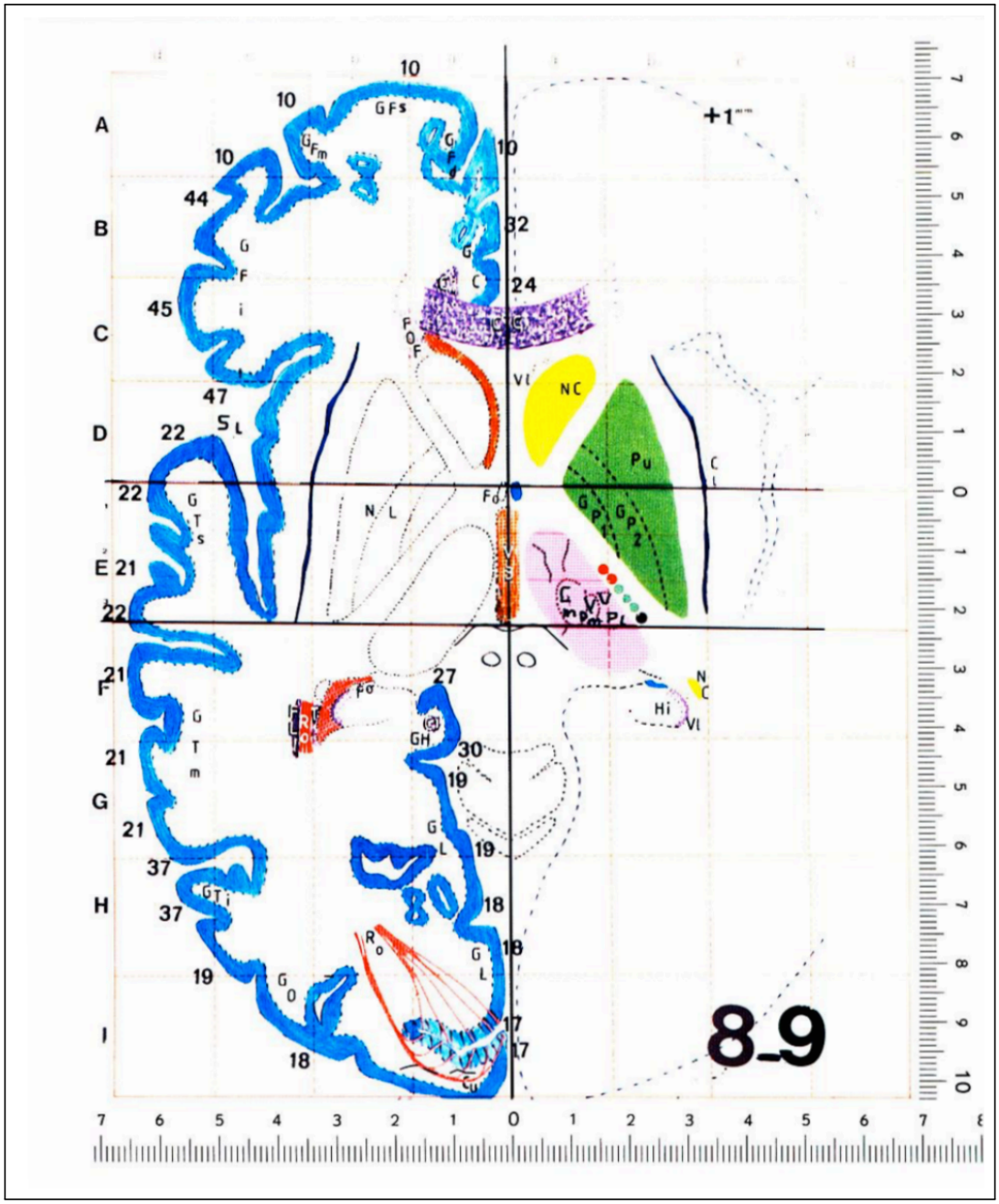

Figure 1.2: The Talairach & Tournoux atlas from 1988. The different parts of the cortex are labelled with Brodmann area numbers. Published with permission from publisher.

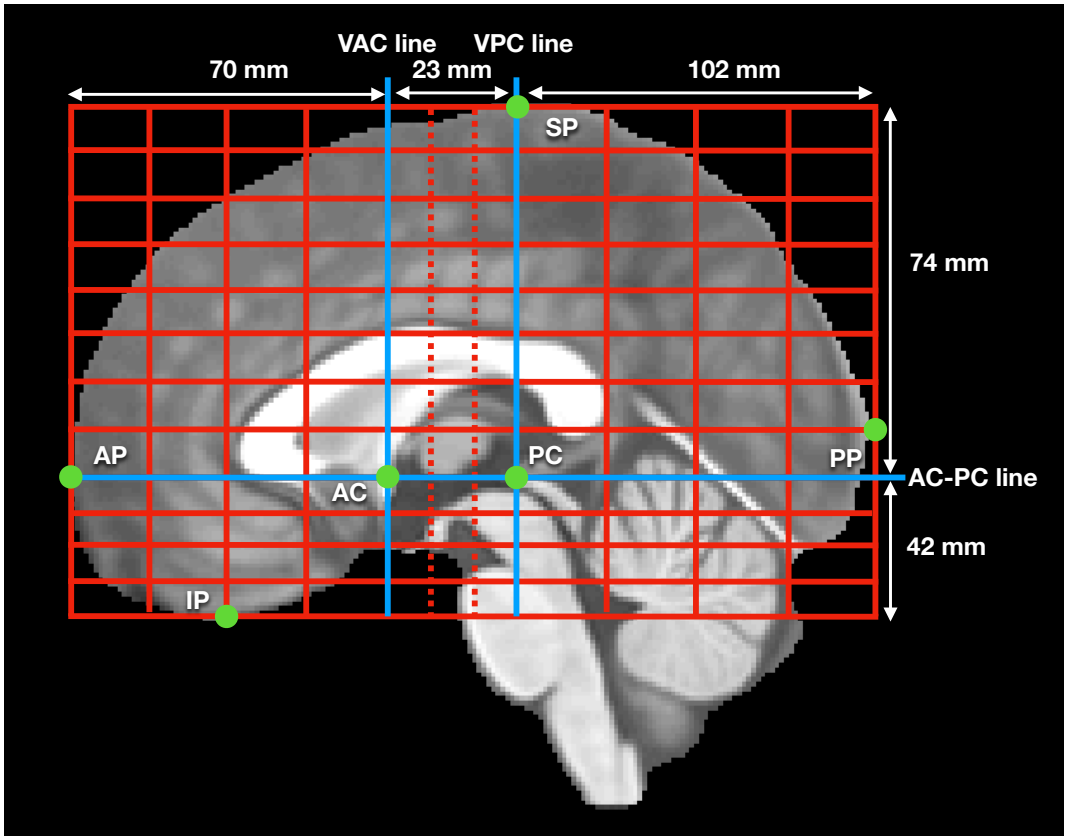

Figure 1.3: The Talairach proportional grid, applied on the MNI brain template.

The reason was that the T1-weighted MRI had a better resolution and better contrast. In T1-weighted images, the GM appears as grey and WM appears as white. This makes it easier to identify different brain structures and landmarks. These landmarks were then transformed over to the PET images of the same subject and then used to linearly resample the PET images to Talairach space. The transformation allowed to translate, scale, rotate, and shear the images globally, but did not involve any local adjustments of brain structures.

The procedure by Evans with colleagues still required manual labelling of landmarks to transform the data into Talairach space. However, if an MRI of a brain already existed as a "brain template" in a standard space, it would be possible to automate that procedure. Such a brain template would preferably be located in Talairach space so that scientists could continue to report 3D foci of functional activations in the same space. Automated algorithms could then be used to transform an individual brain to template space. This involves finding the parameters of a 4×4 transformation matrix A such that a given 3D coordinate v in native space (subject space) is transformed to the new 3D coordinate v' in template space:

$$v' = Av \tag{1.1}$$

where $v = (x, y, z, 1)$ and $v' = (x', y', z', 1)$. This is known as an affine transformation, as it allows for 3 translations, 3 rotations, 3 scaling factors and 3 shears. Obtaining the optimal parameters for matrix A to move from the subject's native space to template-space is called "registering" the image to another coordinate space. Optimisation algorithms can automate this procedure based on the information available in the images. If one image is to be registered to another image of the same subject (e.g., PET to MRI), only 6 parameters (3 translations and 3 rotations) are needed. This is known as a rigid registration, as it does not allow rescaling or shearing of the brain. The number of parameters is often called the degrees of freedom.

In the beginning of the 1990s, two different groups started to work on computerised atlases with the aim to create a brain template in Talairach space; the Human Brain Atlas (HBA) (Roland et al., 1994) and the Montreal Neurological Institute (MNI) atlas (Evans et al., 1993). These new templates consisted of either a single MRI of a brain or an average of many MRIs. They are sometimes referred to as a "standard brain".

The standard brain of the HBA was a single young male brain that deviated the least from a cohort of 20 other male brains. It was furthermore scaled very accurately according to the definitions of the Talairach space, deviating within just a few millimetres. As such, it was assumed that any transformation of brain images to the HBA would remain in Talairach space. The MNI atlas took a different approach. The first version, the MNI305 T1 template, was constructed by first manually identifying Talairach landmarks in 241 young healthy individuals and transforming them to Talairach space using a linear regression to construct a first pass, manually derived, and averaged T1-weighted MRI template. In the second step, 305 brain images were automatically mapped to the average template with a 9-parameters linear transformation, which would further reduce manual errors induced in the first pass.

The Talairach atlas and corresponding Talairach space had a number of limitations for brain research. Since it was based on the post-mortem brain of a 60-year old female, which deviated heavily from what we would consider a representative brain of the population, almost any mapping to this space would result in a large anatomical deviance. The piecewise linear mapping was employed to overcome some of the non-linear anatomical differences. However, this piecewise linear mapping was difficult to apply for resampling brain images. While still a useful approach for surgery, piecewise linear mapping was therefore not well-suited for brain imaging research.

The MNI305 was therefore only a linear approximation to Talairach space and it turned out that the remaining non-linear anatomical variability would cause the template to be larger than the typical brain. It is therefore referred to as MNI space rather than Talairach space (Brett et al., 2002). This also had an advantage. This meant that the MNI space would become more representative of the population as it is not locally deformed to perfectly match the Talairach atlas.

This approximation has unfortunately given rise to confusion in the neuroimaging field, where coordinates in MNI space have sometimes been reported as Talairach coordinates. At the same time, research groups using the HBA would also report their findings in Talairach space, even though a linear transformation to the HBA template would also be just an approximation.

A number of atlases that are based on the MNI305 atlas have been created. In 1998, the Colin27 atlas was published which was based on an average of 27 MRI scans from one individual that was linearly transformed to the MNI305 template (Holmes et al., 1998). The ICBM152 template (International Consortium for Brain Mapping) was created in 2001 as the average of 152 brain images with the benefit of being in a higher resolution than the original MNI305 template (Mazziotta et al., 2001a,b). The ICBM152 template also came with probability maps for GM, WM, and cerebrospinal fluid (CSF). These images were still only linearly mapped to MNI305, making the template a bit fuzzy since the linear mapping only adjusts the brains on a global scale and not locally. For instance, two brains that have the same total brain volume may still have differences in some local brain structures, both in shape and size.

The affine transformation that is used to linearly transform coordinates from one space to another space can be complemented with non-linear transformations. There exist a number of different methods to perform non-linear transformations, including polynomial warps, cubic B-splines, local translations, and discrete cosine transforms (Klein et al., 2009). By using a non-linear transformation to warp the individual brain images to standard space, it is possible to create a non-linear template. The procedure is repeated a number of times, where for each iteration a more detailed non-linear template replaces the previous version. This procedure was used to create the non-linear ICBM152 template. A first version was released in 2006 and a refined version was released in 2009 (Grabner et al., 2006; Fonov et al., 2009).

Figure 1.4 depicts some of the various templates that have been developed throughout the years. The procedure for using these templates can vary, but are essentially as follows: The functional images for an individual are registered linearly to the T1-weighted MRI image of that individual (often using 6 degrees of freedom in the transformation calculation to allow rotation and translation but not scaling) and the T1-weighted image is in turn registered linearly to the template (often using either 9 degrees of freedom or 12 degrees of freedom, to also allow scaling in all directions separately and also shearing). This allows all the functional images to be linearly transformed to MNI space as accurately as possible.

Having transformed the images into a common space, one can assume that a given voxel with a given MNI coordinate is approximately describing the same position in different brains. To further improve the transformations, non-linear transformations that would allow for local changes can also be used.

1.2.4 Computerised regional atlases

In 1983, two different groups worked independently on computerised regional atlases, both with the idea to construct a system to automatically locate and measure local anatomical structures in brain images, such as the thalamus and the basal ganglia. Both systems worked similarly by the use of a predefined atlas that could be non-linearly warped to the image of a subject's brain (Bohm et al., 1983; Bajcsy et al., 1983). The system by Bohm and colleagues was further developed and later called the Computerized Brain Atlas (CBA) (Bohm et al., 1991).

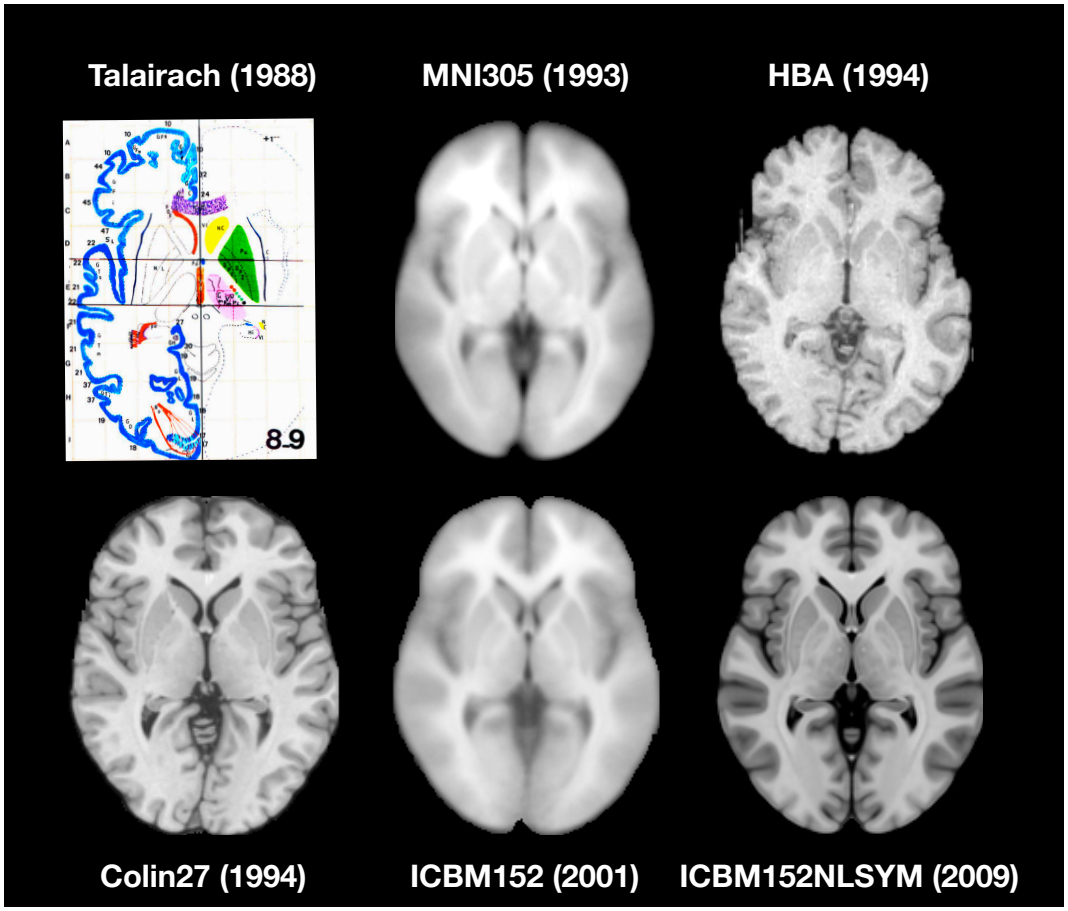

Figure 1.4: A comparison between the printed Talairach atlas, the MNI305, the HBA, the Colin27, the ICBM152, and the non-linear and symmetric ICBM152.

Neither system seemed to have used the Talairach coordinate system, but the landmarks used in the CBA were at least similar to the Talairach landmarks. Both systems were designed to run on a VAX-11/780 minicomputer, which was a very expensive and big computer available to relatively few. These were very specialised systems. Hence, it wasn't really possible to share these atlases with the larger scientific community. This was maybe the main reason why these early computerised atlases never got established as a standard. The printed Talairach atlas was much more accessible for most researchers and around 1985 it was already getting established as a common space to report findings (Fox et al., 1985). The HBA and MNI templates would make this procedure even easier.

However, note that the HBA and MNI templates shown in Figure 1.4 do not have any labels. It is the analogue of having a world atlas without any delineations between countries or labels describing points of interests. For more detailed information about a certain coordinate, such as which Brodmann area that it belongs to, it was for a long time necessary to look it up using the printed Talairach atlas. To automate this procedure, Lancaster with colleagues developed a tool that they called the Talairach Daemon, which consists of a database with 3D coordinates where researchers can enter the Talairach coordinates and get back a hierarchical list of labels from the Talairach atlas including the Brodmann areas (Lancaster et al., 1997). Nevertheless, since the coordinates are entered in Talairach space, a transformation between MNI and Talairach space has also been proposed to correct for bias between the two spaces (Lancaster et al., 2007).

Mapping the Brodmann areas to a standardised 3D space from Brodmann's own drawings (see Figure 1.1) was for obvious reasons not a very accurate procedure. Amunts et al. (2020) therefore created a modern computerised cytoarchitectonic atlas based on 23 postmortem brains, which were transformed to both the single subject MNI-Colin27 template and the 2009 version of the non-linear and symmetrical ICBM152 template. These have been released as part of the JuBrain Anatomy Toolbox (Eickhoff et al., 2005). Atlases for gross anatomical structures have also been constructed, in which the automated anatomical labelling (AAL) atlas is one of the most used ones (Tzourio-Mazoyer et al., 2002). Figure 1.5 shows an axial view of the Talairach Daemon, the JuBrain, and the AAL atlas (version 3) in comparison to the printed Talairach atlas.

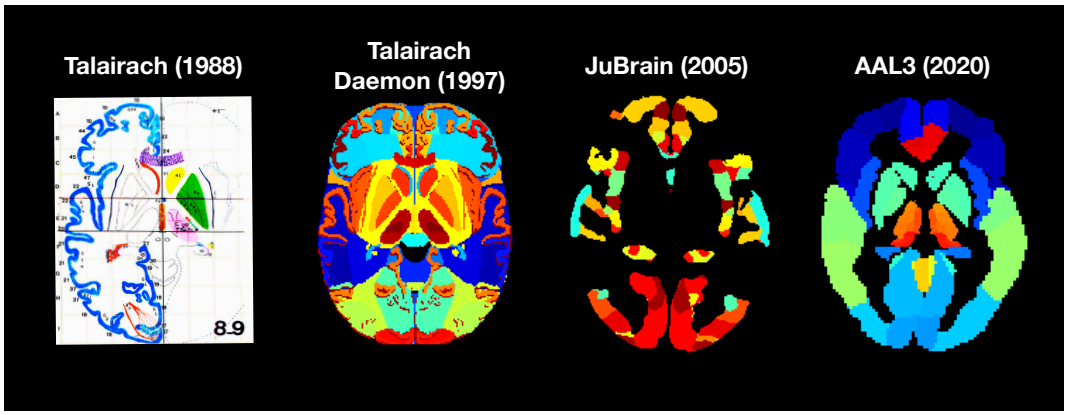

Figure 1.5: From left to right: The printed Talairach atlas, the Talairach Daemon, the JuBrain Anatomy Toolbox, and the AAL atlas (version 3).

Lancaster described two different procedures for using a regional atlas (Lancaster et al., 1997). The forward-transform method is the one used by the Talairach Daemon, where the regional information can be obtained for coordinates in standard space. The other method is called the inverse-transform, where a region is transformed from the atlas to the individual brain (or another template space) in order to obtain the volume of the given region in that space. By combining it with the individual's tissue segmented maps (GM, WM, CSF), it is possible to get fairly accurate regional volume information on an individual level (Collins et al., 1999).

Most regional atlases are nowadays constructed for either the ICBM152 or the Colin27 templates, which are templates of young adults. This includes the JuBrain atlas and the AAL atlas. However, age is one of the factors that correlate with brain size. The brains of older individuals have often cortical atrophy and larger ventricles compared to younger individuals (Blinkouskaya and Weickenmeier, 2021). This makes a template of younger adults less ideal as a transformation target for ageing studies. The warping algorithm will in that case need to reduce the size of the ventricles and reverse the cortical atrophy in order to match the younger template – in a sense reversing the ageing process in order to match the older brain to a younger template space.

The aim of **Study I** was therefore to develop an old brain template (average age 75 years) with corresponding tissue atlases and a regional atlas to be used for ageing studies, called the AGES atlas (from the Age Gene/Environmental Susceptibility-Reykjavik Study). This would reduce the deformations required to warp from native space to template space or vice versa. The tissue atlases would also allow the calculation of a deformation field between the AGES template and other study specific tissue templates, making it possible to warp the atlas to other study cohorts.

1.3 Functional brain imaging

1.3.1 Measuring brain activity

In the late 1870s, Angelo Mosso hypothesised that cognitive tasks can increase cerebral blood flow locally in the brain. This hypothesis was tested using a device that could measure changes in cerebral blood flow on patients with skull defects by recording brain pulsations. He continued his work by developing the 'human circulation balance', a device that could measure the redistribution of blood in the body for healthy subject with the skull intact during emotional and intellectual activities. William James, who was interested in blood flow variations of the brain, reported Mosso's findings in his book that was published in 1890 (Sandrone et al., 2014). The same year, Roy and Sharrington hypothesised a connection between neural activity and cerebral blood flow due to cerebral oxygen consumption (Roy and Sherrington, 1890).

However, it would take many years before someone would investigate this experimentally again. The first study to report quantitative measurements of the total blood flow to the brain was published by Kety and Schmidt (1945). Their technique used nitrous oxide to measure global cerebral blood flow. Some years later, in 1961, an early technique that allowed the measurements of rCBF in animals used the radioactive noble gas krypton^{85} that would follow the blood flow and emit low energy β-radiation. This radiation was measured locally using a Geiger-Müller tube and craniotomy was needed to allow the tube to get close to cortex of the brain. The signal was then recorded with an ink-writing plotter (Lassen and Ingvar, 1961). In 1967, a similar principle but with the skull intact was applied in humans where four detectors at different locations measured rCBF using a xenon^{133} isotope, demonstrating an increase in rCBF during mental effort (Ingvar and Risberg, 1967).

In 1973, computer technology allowed for an even more advanced study using 32 detectors. This study demonstrated a difference in rCBF patterns between two psychological tests and a rest condition where the subject did not perform a specific task (Risberg and Ingvar, 1973). This was probably one of the first digitised studies of rCBF changes in the human brain. It did not provide images of brain activity, but had at least had a grid of detectors that covered the brain sagittally. This kind of technology was enhanced a few years later, with a digital gamma camera technique consisting of 254 detectors that could provide true imaging (Roland and Larsen, 1976). This early technique only allowed to measure a 2D image of the brain, for instance as a sagittal view in which case the signal could either come from the left or the right hemisphere.

Obtaining a true 3D volume of the rCBF in the brain (with voxels – the 3D equivalent of a pixel – as the element of measurement) first became possible with the PET scanner. In 1983, Raichle with colleagues demonstrated that by using $H_2\,{}^{15}O$ as an intravenous radio tracer, it was possible to measure rCBF using the PET scanner. The radio tracer was injected in the subject's blood stream and when it decayed, a positron (the anti-matter of an electron) was emitted. Once it would hit an electron, both particles would annihilate and be replaced by two photons travelling in opposite directions, each with an energy of 511 keV (Herscovitch et al., 1983; Raichle et al., 1983). These coordinated gamma pulses would then be observed by the detectors in the PET scanner. Computer algorithms were used to reconstruct the 3D location of the decay.

This radio tracer has a half life of 122 seconds, so a typical experimental setup could be to measure one scan every 5 minutes while the subject would repeat a task throughout the scan. The contrast between the task and the rest condition would then reveal which areas in the brain that had an increased rCBF during the task. This kind of design is typically known as block design, since each task is repeated for many seconds during the scan.

During the late 1980s and the beginning of the 1990s, PET imaging remained the most common non-invasive technique to measure local brain function. However, in 1990, functional MRI (fMRI) was invented. This allowed the use of the MR scanner to measure increased neural activity through changes in oxygenation concentration using the so called Blood Oxygen Level Dependent (BOLD) contrast. This contrast uses the blood itself as a contrast agent without the need of injecting an intravenous contrast (Ogawa et al., 1990; Glover, 2011).

Functional MRI also allowed a higher temporal resolution of just a few seconds, which should be compared to 5 minutes with PET. Although many fMRI studies still apply block design (where the task is repeated for a number of seconds), the higher temporal resolution opened for so called event related design where the timing of an event could be modelled in the experiment (Friston et al., 1998). Nowadays, fMRI is the most common imaging technology to measure brain activity.

1.3.2 Functional connectivity

In task related studies, a typical approach could be to contrast a test condition (for instance, move the right hand) with a rest condition at a voxel level. The result would then show which voxels in the brain that are more active in hand movement compared to a resting state.

Voxels that are co-activated during the same task may also be functionally connected. In 1993, Friston with colleagues defined functional connectivity as *the temporal correlation between neurophysiological (functional) measurements made in different brain areas*. By applying Principal Component Analysis (PCA), they demonstrated how a data mining approach could automatically identify functionally connected regions commonly involved in a verbal fluency task, based on a large set of PET images (Friston et al., 1993).

The poor temporal resolution in PET does not make it possible to directly measure temporal correlations. We can just assume that the co-activations seen in PET have a temporal relationship. However, this is possible with fMRI. By using a seed voxel approach, Biswal et al. (1995) demonstrated from resting state images that a voxel known to be activated in a finger-tapping task also correlated with a primary motor cortex network at rest. The voxel that is chosen as the source is called a "seed voxel". The temporal signal from this voxel correlated with voxels in the motor cortex but remained uncorrelated with other voxels, even when the subject was resting. This was an indication that the network continued to have spontaneous fluctuations in the BOLD signal even at rest.

A few years later, Raichle et al. (2001) demonstrated the existence of a default mode state of the resting brain, where some regions (including anterior cingulate cortex and posterior cingulate cortex) showed greater activity at rest compared to cognitive demanding tasks. This work was followed by Greicius et al. (2003), who demonstrated an inverse correlation between the posterior cingulate cortex and three lateral prefrontal regions using seed based analysis in resting state fMRI. A further investigation of the spontaneous BOLD signal fluctuations was done by Fransson (2005), who found that the brain at rest toggles between different states, a state-of-mind state and an extrospective state, rather than having a single default mode state. This was done by looking at the actual frequencies of the BOLD signal. A similar result was shown by Fox et al. (2005), who demonstrated an intrinsic organisation of an attention-demanding network that continues to have spontaneous fluctuations even at rest and that is anti-correlated with a default mode network.

A third approach to investigate spontaneous fluctuations was introduced by Beckmann et al. (2005), who used Probabilistic Independent Component Analysis (PICA) to demonstrate the existence of eight distinct brain networks including the default mode network. Fransson et al. (2007) further showed the presence of five unique and spontaneous intrinsic brain activation networks in infants using PICA analysis. A correspondence of these networks with functional brain maps from task related experiments was shown by Smith et al. (2009), demonstrating that explicit activation networks continue to be temporally correlated by spontaneous activations even at rest.

Graph theoretical approaches have also been used to study functional connectivity. These methodologies analyse patterns of covariation at a large scale by mapping brain activity to a graph with brain regions corresponding to “nodes” and the significant correlations between them to “edges”, i.e. links between nodes (see Figure 1.6). From such graphs, a number of different metrics can be obtained. The simplest metric is “degree centrality”, which represents, for each node, the number of connected nodes. Nodes that have a high degree centrality are known as hubs. More advanced metrics are the shortest path length between two nodes and the average distance between one node and all the other nodes (Rubinov and Sporns, 2010). The results can also be represented as a matrix. It is common to divide the brain into a limited set of regions to keep the number of nodes low since the calculations are computationally heavy (e.g., 100 nodes) (Evans, 2013).

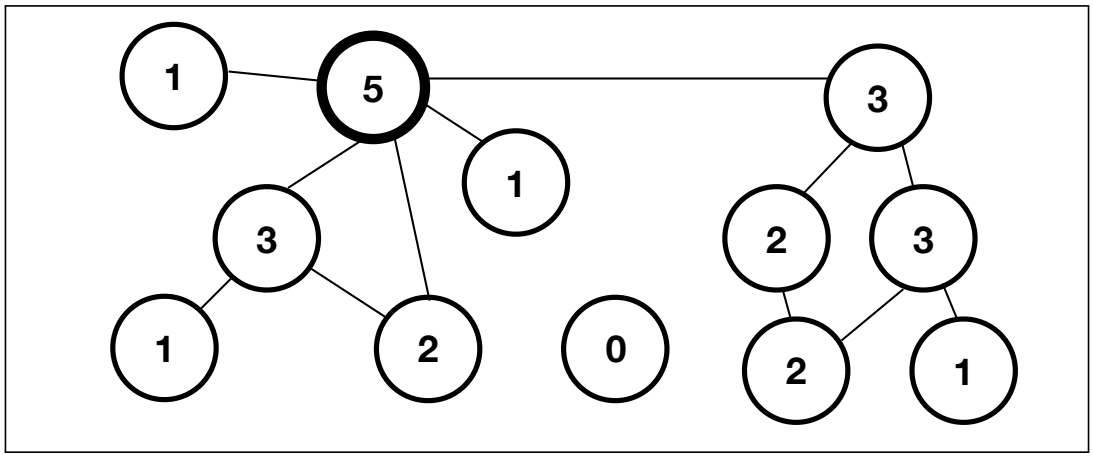

Figure 1.6: An example of a graph, where the nodes may represent regions or voxels depending on the level of granularity and the edges between the nodes represent significant correlations. The number in each node represents the number of connections to the other nodes in the graph, known as "degree centrality" in graph theory. The node depicted in bold has the highest level of "degree centrality" with 5 edges connecting to other nodes, and is therefore considered as a hub.

Graph theory can also be used with each voxel as a node, but is then often limited to only measure the degree of functional connectivity due to the complexity of the computations. By calculating an $n \times n$ correlation matrix, with n number of voxels, and then counting the number of significant correlations for each voxel at a given threshold, it is possible to obtain a connectivity degree map that is reflecting the functional global brain connectivity (fGBC) at each voxel.

Some voxels will have a higher fGBC during resting state, depending on which networks they belong to. This was first demonstrated by Buckner et al. (2009), who also showed that the hub regions are vulnerable of amyloid-β deposition in Alzheimer’s disease using PET amyloid imaging. This procedure was also used to demonstrate that voxels within the default mode network and the cognitive control network have a high level of fGBC (Cole et al., 2010).

1.4 Structural volumetric imaging

1.4.1 Voxel-based morphometry

The need for a standard coordinate space in brain imaging was originally to allow consolidation of functional information across individuals so that a group level result could be obtained. The aim was therefore to minimise inter-individual differences in both shape and size to remove anatomical differences.

It was not until 1995 that Wright with colleagues published a work that described how to characterise differences in GM and WM between individuals with schizophrenia in a standard space at a voxel-by-voxel level (Wright et al., 1995). The method segmented out GM and WM as separate maps from the T1-weighted images, filtered the maps with a spatial filter, and transformed them into Talairach space. A general linear model (GLM) was used at a voxel level with GM and WM density as dependent variables and syndrome score as independent variable along with confounding variables (age and sex). The results showed a significant relation between severity of symptoms and tissue density. The procedure used to quantify differences in local tissue density at a voxel level was later called voxel-based morphometry (VBM).

An optimised VBM method was presented in 2001, where a non-linear GM study specific template was created based on the study material and the GM map from each individual was non-linearly transformed to this template (Good et al., 2001). Since such a transformation could either result in local expansion or contraction, the optimised procedure would adjust for this so that the total GM would remain the same (by dividing the GM voxel values with the scaling factors). This study investigated GM loss both globally and locally with increasing age and found both a global loss of GM as well as an accelerated regional loss in specific areas.

1.4.2 Structural covariance

The same methods that are used in functional connectivity, such as seed voxel analysis, can also be used to study GM covariance between individuals. This was first demonstrated in a study by Mechelli et al. (2005), where they used a VBM seed voxel approach to demonstrate that the GM density in 12 different regions indeed covary with other regions across individuals. This is not at all a given fact. As the authors explained, an alternative outcome could have been that the GM density topography is unique for each individual, in which case there would be no shared variance between voxels across individuals. Their result showed the opposite, for instance that a seed voxel in the left amygdala will correlate not only with other voxels within the left amygdala but also with voxels within the right amygdala and vice versa across individuals. Consequently, this also means that if an individual has a high GM density in voxels within the left amygdala, it will probably also have a high GM density in voxels within the right amygdala.

The results from Mechelli et al. (2005) also demonstrated that different seed voxels may have a different number of significantly correlated voxels. **Study II** investigated this further in an older population (68 to 83 years) by raising the question if there are specific voxels that covary to a larger extent with many other voxels by using every single GM voxel as a seed voxel and counting the number of significant correlations ("degree centrality" in graph theory).

The technique used in **Study II** resembles the one used for fGBC, but in this case it was used to measure the degree of structural covariance. We called this the voxel's level of structural covariability. Relating back to ageing as one of the contributors to morphological differences, this study compared the resulting covariability maps between two different age groups (68-77, 78-83).

Study III investigated further if a similar covariability map would emerge in a much younger population with age range 18-35 years. Since GM density removes any effects of global brain size, **Study IV** looked at the differences in covariability between GM density and GM volume for the younger population.

Another way to investigate GM covariance patterns is to use ICA in combination with VBM to determine separate sources of covariation within GM structure. This was done in a study where they identified five different sources that covaried with different aspects of the brain. The authors discovered that the GM densities were greater in healthy controls compared to schizophrenia patients in all sources (Xu et al., 2009). These sources consisted of variations in a) the temporal GM, b) the thalamus, c) the basal ganglia, d) the parietal GM, and e) the frontal/temporal GM. A similar analysis using ICA on GM showed that structural variation at some level mapped onto the functional organisation of the brain (Smith et al., 2019). However, another study only identified a limited relationship between functional connectivity and structural covariance by looking at nine seed regions (Reid et al., 2017).

Study III therefore explored to which extent the full correlation matrix of inter-individual GM densities overlapped with a corresponding functional correlation matrix, after thresholding at a significance threshold level.

A similar method to ICA is to use unsupervised autoencoders to obtain non-linear latent factors in a dimensionally reduced latent space that still explains most of the variance. An autoencoder is an artificial neural network with two parts. The first part is called the encoder, which learns to represent brain images in the latent space. The second part is called the decoder, which learns to reconstruct the same brain images from the latent space. Therefore, when training the autoencoder, the input of the neural network is the same as the output, while the middle layer consists of only a few neurons representing the latent factors. This technique was used in a study to find relations between cognitive symptoms and neurodegenerative processes in the latent space (Martinez-Murcia et al., 2020).

In **Study IV**, a variational autoencoder was used to discover the number of latent dimensions that are required to reproduce a majority of all significant GM volume correlations between all voxels. A variational autoencoder is similar to an autoencoder, but maps the input to a multivariate latent distribution and is less prone to overfit (Kingma and Welling, 2013). The correlations between the latent factors and GM structure were obtained in a VBM analysis to see how these correlations were related to the covariability hubs. The latent factors were also correlated to phenotypic variables such as sex, age, and fGBC.

2 Aims

This thesis aims at answering a number of fundamental questions regarding brain structure variability and its relation to age.

Study I: The aims were to develop a non-linear brain template and a corresponding regional atlas for ageing studies, together with a regional segmentation analysis procedure to study how well it could account for individual morphological differences. Ageing brains are affected by gross morphological changes over time, making brain templates and atlases from younger cohorts less ideal for ageing studies.

Study II: This study aimed at investigating how ageing brains differ in GM and especially if there are core differences that are coordinated between brain regions, by studying GM correlations between brain voxels in a study cohort between 68 to 83 years. Since the brain goes through gross morphological changes over time, the question was also if such core differences in an ageing population would be explained by the age differences or if these core regions have a totally different origin.

Study III: To further understand the core of the coordinated variations, the aim was to see if the core differences within a younger cohort of young adults between 18 to 35 years would be similar or different from those of an older cohort. Furthermore, the study also investigated to what extent patterns of structural covariation at the group level corresponded to patterns of functional connectivity seen during resting state.

Study IV: The fundamental core of structural covariance could either be the result of a few unknown factors or the result of many different factors. The aim of this study was to investigate if the core hubs of structural covariance could be reproduced in a low-dimensional latent space or require a high-dimensional latent space indicating a heterogeneous interplay between many factors.

3 Methodological proceedings

3.1 Study materials

The participants in **Study I** and **Study II** were randomly selected from the AGES-Reykjavik Study cohort, which consists of 5764 participants where 4811 underwent MRI (Harris et al., 2007; Sigurdsson et al., 2012). In **Study I**, the aim was to build a template and a regional atlas for ageing studies, called the AGES atlas. With the purpose of being representative for the whole study cohort, 400 individuals were selected randomly from the 4811 individuals with MRI (T1-weighted, (PD)/T2-weighted, and FLAIR), and 86 individuals were subsequently removed due to poor image quality or having too large brain infarcts. The remaining 314 individuals were considered to be a representative subsample of the whole cohort. These were used to construct the template and atlas (mean age 75 years, age range 66 to 92 years, 60 % women). Cases with dementia and mild cognitive impairment were also included if they were selected by the random selection process.

In **Study II**, the aim was to investigate structural covariance in a healthy older cohort with a balanced distribution of age and sex. For each year of age between 68 and 83 years, 30 men and 30 women without dementia or larger infarcts were randomly selected, giving 960 individuals in total.

In **Study III** and **Study IV**, where the aim was to further investigate structural covariance in a younger cohort, the control group of young adults from the publicly available dataset ABIDE was selected (Martino et al., 2014). Individuals with an age between 18 to 35 having a measured Full Scale IQ (FIQ), resting state fMRI, and T1-weighted images, were included giving 138 individuals in total (19 women, 119 men).

3.2 Making the AGES atlas: Study I

3.2.1 Pre-processing

All MR images had previously been processed through a tissue segmentation pipeline, where T1-, T2-, PD-weighted, and FLAIR images were used as input to a tissue segmentation classifier (Sigurdsson et al., 2012). Each voxel was classified into either GM, normal WM (NWM), CSF, or WM hyperintensities (WMH). White matter was then regarded as the sum of NWM and WMH.

3.2.2 Constructing the symmetric templates and tissue atlases

Four templates were constructed, one for each image sequence (T1-, T2-, PD-weighted, and FLAIR). The procedure started with a linear transformation to MNI space, where an initial linear T1-weighted template was constructed by averaging all the individual images in MNI space. The aim was to construct a symmetric template, so each image was also left-right flipped and averaged with itself.

After this first phase, all T1-weighted images were non-linearly transformed to the linear template using the ANIMAL tool (Collins and Evans, 1997), where a new symmetric non-linear template was constructed. This registration/averaging procedure was repeated a number of times to improve the template for each generation. For the first two generations, both the source images and template were blurred using a Gaussian kernel with a full width at half maximum (FWHM) of 8 mm. The early generations had a large spatial filter, which then decreased with increasing number of generations to give a range from 8 mm for the first generation to 1 mm for the last generation. The same level of blurring was repeated twice for the early generations and four times for the last generations. A total of 16 generations were constructed, with 5 different levels of blurring. The template was called the AGES314 template.

The subject-to-template deformation fields obtained from the final generation were then used to also construct the corresponding T2-, PD-weighted, and FLAIR templates, using the same procedure of mirroring and averaging the individual images in template space. The same procedure were used to construct tissue atlases (CSF, GM, WM, WMH), by warping each individual's tissue segmentation to the template space and then mirroring the tissue maps before averaging the results.

3.2.3 Constructing the regional atlas

The aim of the regional atlas was to construct a gross anatomical atlas, for which all major cortical structures (frontal GM/WM, temporal GM/WM, etc), all major structures in deep GM (the thalamus, the basal ganglia, etc), and ventricles were included, giving a total of 56 anatomical regions.

An application written for Mac OS X was developed to allow manual labelling using a Wacom tablet. It allowed the user to follow the borders from the tissue segmentation or draw freehand, depending on the region. This helped the user to optimise the labelling process, but it would still take a week to manually label one brain. In whole, seven subjects were labelled, where four were used to construct the regional atlas and three were used to validate the atlas using a regional segmentation pipeline.

In a first phase, the manually labelled images from the four subjects were warped to the non-linear template and subsequently mirrored. Each region was warped separately to template space. In template space, an initial max-likelihood atlas was constructed. This atlas was then warped to all the 314 template subjects for an initial regional segmentation. The tissue maps of the individual template subjects were used to constrain the segmentation, so that e.g. WM voxels would not be classified as GM regions.

In the second phase, the results were warped back to template space where a max-likelihood regional atlas for each tissue (GM, WM, CSF) was constructed. Some regions, such as the thalamus and the globus pallidus, contain both GM and WM structures and were therefore added to both the GM and WM regional atlases.

3.2.4 Validation using a regional segmentation pipeline

The size of the regions matter. If the regions are too small, the performance of an automatic regional segmentation algorithm will be poor. In order to validate this, the three manually labelled subjects that were not used in the creation of the atlas were regionally segmented using the regional atlas. The manually labelled regions were then compared to the automatic segmentation.

The procedure of the regional segmentation is shown in Figure 3.1. Each regional tissue atlas was warped to the individual subject where it was multiplied with the corresponding tissue mask of the subject (for instance, the regional GM atlas was multiplied with the subject's GM mask). The sum of the masked regional atlases in subject space gave the final output.

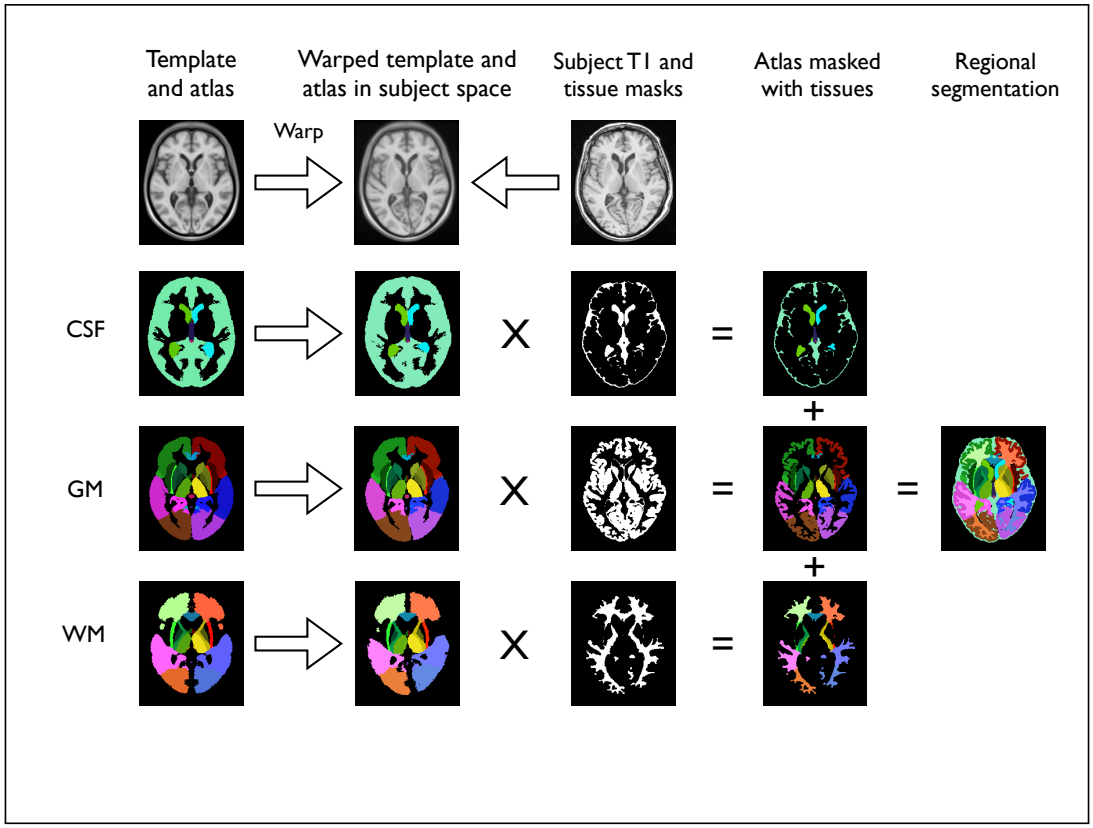

Figure 3.1: The regional segmentation of a subject starts with warping the template to the subject space. The deformation field is then used to separately warp the regional tissue atlases to subject space where they are multiplied with the tissue masks of the subject. The results are summed together to form a final regional segmentation of the subject.

For each region, the accuracy of the segmentation was tested by calculating how well the manually labelled regions overlapped with the automatically segmented regions. This was done using the Dice Similarity Coefficient (DSC), which gives a measure between 0 and 1 depending on how well they overlap (0 means no overlap, 1 means perfect overlap) (Zijdenbos et al., 2002). The reproducibility of the regional segmentation was also validated using data from 31 subjects with two different visits. Within-subject Coefficient of Variation (CV), between-subject CV, and DSC were calculated for each region. The Index of Individuality ratio (IoI) was also calculated as the ratio between the within-subject and between-subject CV.

3.3 Analysis of structural covariance: Study II - IV

3.3.1 Tissue segmentation

In **Study II**, the MR images were processed through a tissue segmentation pipeline that separated each brain into CSF, GM, WM, and WMH. This pipeline was specifically developed for the AGES-Reykjavik Study to consider WMH as a separate tissue class and is described in detail by Sigurdsson et al. (2012). In **Study III** and **Study IV**, the MR images were tissue segmented into CSF, GM, and WM using the FSL tools (Smith et al., 2004).

3.3.2 Voxel-based morphometry pre-processing

The VBM procedure was performed separately for the **Study II** cohort and for the **Study III** and **Study IV** cohort. The GM maps obtained from the tissue segmentation were first warped to the MNI-ICBM152 2 mm isotropic template, where a study specific symmetric GM template was created. This template was used as a non-linear target to warp the GM maps to the template. The GM maps were then corrected for local expansions and contractions, resulting in GM maps representing the GM density of each voxel.

For **Study IV**, maps representing GM volumes were also calculated. This was done by first calculating the scaling factor from subject space to template space and then dividing it with the GM density map. In **Study II**, the GM mask consisted of 207110 voxels. For **Study III** and **Study IV**, the GM maps were subsampled to the same resolution as the resting state fMRI-images in MNI space (3 mm isotropic), giving a GM mask of 79187 voxels.

3.3.3 Calculate covariability maps

Given a GM seed voxel, either from GM density or GM volume maps, and a significant threshold T, we can calculate a brain map that describes how well this seed voxel correlates with all the other GM voxels in the brain across a large set of individuals. Some seed voxels will only correlate significantly with a few other voxels, whereas others will correlate significantly with many voxels. In these studies, we called this the voxel's covariability level, indicating to which extent it covaries with other voxels. A large number would indicate that it has a central position in the covariance structure. Regions with a high covariability level are therefore regarded as hub regions. Figure 3.2 demonstrates how the level of covariability can differ between two different seed voxels from **Study II**.

A covariability map of the whole brain can be obtained by using each voxel as a seed voxel to calculate the number of significant correlations per voxel. In practice, this is done by first calculating the correlation matrix between all voxels and then thresholding the matrix at the threshold level T. The sum of all rows then gives, for each column, the number of significant correlations. In **Study II**, this matrix had the size 207110×207110. For **Study III** and **Study IV**, the matrix was smaller with the size 79187×79187.

A permutation analysis can be used to obtain the significant threshold T. In **Study II**, this was done by permuting the order of the subjects in the seed voxels 5000 times, resulting in 5000 permuted correlation matrices, each of size 207110×207110, from which the maximal false correlation for each permutation can be obtained to get a distribution of the null-hypothesis. The obtained thresholds were $T = 0.54$ at $p = 0.001$ and $T = 0.45$ at $p = 0.05$.

In **Study III** and **Study IV**, the threshold $T = 0.54$ was reused and a permutation based false discovery rate procedure was used to validate that the threshold was still significant at $q < 0.05$ (allowing up to 5% false positive voxels among the true positives), even though there were fewer subjects.

In **Study II**, the study cohort was also subdivided into four different groups (men between 68-75, women between 68-75, men between 76-83, and women between 76-83). The covariability maps within each group were calculated. A permutation analysis between the groups was done to find out if one group had a significant different covariability level than any other group.

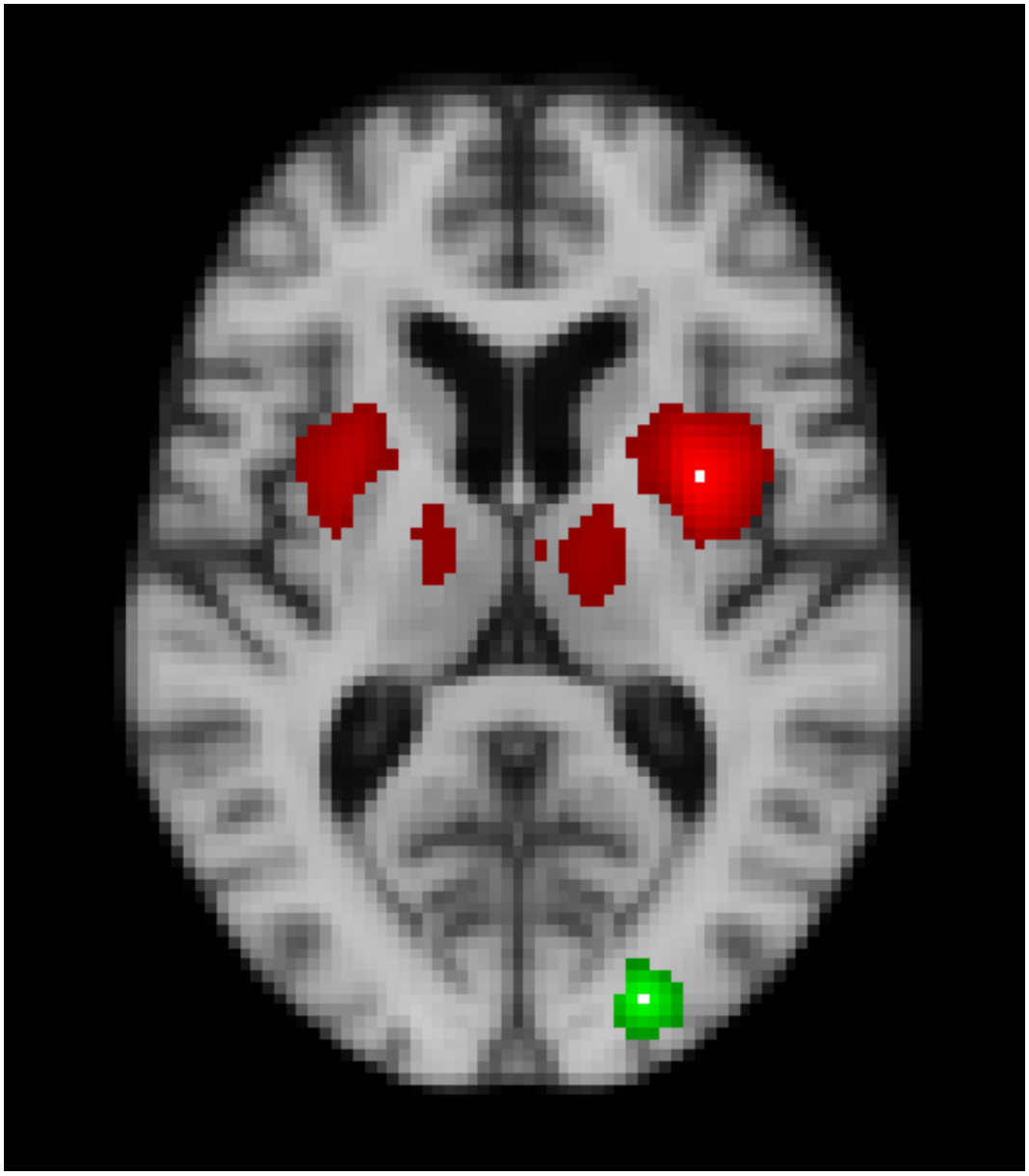

Figure 3.2: Two examples of seed voxels from **Study II**, where the seed voxel in the occipital lobe gives rise to a green correlation pattern of 125 significantly correlation voxels and has therefore a very low covariability. The seed voxel in the putamen gives rise to a red correlation pattern of 2331 significantly correlating voxels and has a high covariability. The two seed voxels are depicted as white voxels.

3.4 Analysis of functional connectivity: Study III

In **Study III**, one of the aims was to see how well the structural correlation matrix and the functional correlation matrix overlapped. Under the hypothesis that functional connectivity would be a major causal factor for structural covariance, one would expect a large overlap between the two matrices. The intersection between the structural covariability matrix and the functional connectivity matrix after thresholding gave an intersection matrix telling which voxel pairs that covaried significantly both structurally and functionally. The sum of all rows would then give the shared structural covariability and fGBC level for each voxel. The resting state fMRI data was downloaded from the pre-processed ABIDE data set, which had already been pre-processed and transformed to MNI-space.

The inter-individual functional correlation matrix was calculated by first obtaining the functional correlation matrix for each subjects, Z-transforming each correlation matrix using Fisher's transform, summing together the matrices using Stouffer's method, and finally transforming the sum back to a Pearson correlation matrix where the values could be thresholded at $T = 0.54$. The validity of using the same threshold for functional connectivity was again tested using a permutation based false discovery rate.

3.5 Analysis of structural dimensionality: Study IV

Different seed voxels may give rise to totally different correlation patterns, as is shown in Figure 3.2. However, two correlation patterns obtained from two different seed voxels may also overlap, even if the two seed voxels do not correlate significantly with each other. All voxels within a correlation pattern may be seen as having a common source of variability (genetic or environmental, or both). This raises the question of how many underlying factors – or latent dimensions – that are needed in order to describe a majority of all significant correlation patterns across all seed voxels. These would most likely correspond to external factors of both genetic and environmental origin that capture the major characteristics of inter-individual structural brain covariance.

The first aim of **Study IV** was to use a convolutional variational autoencoder to discover how many latent factors that were necessary to reconstruct the majority of all significant correlations. An autoencoder is a neural network which aim is to generate the input as output, but with a limited number of neurons in the middle layer representing the reduced latent space. The autoencoder was used to reconstruct the images through the latent space to see if the reconstructed images could replicate the covariance patterns at a given number of hidden latent factors.

The second aim was to use the latent factors in a VBM analysis to study how they correlated with GM. These correlation patterns may reveal something about the nature of the structural hub regions. The third aim was to investigate the relationship between the latent factors and functional connectivity, total GM volume, total GM density, age and Full scale IQ (FIQ). The relationship with functional connectivity was explored by calculating a fGBC map for each subject. These were then used used in a GLM with the latent factors as independent variables.

4 Results and general discussion

4.1 Main findings

4.1.1 Study I

All the studies of this thesis focused on different aspects of variance in human brain morphology. Ageing is one important factor behind this variance. The aim of **Study I** was therefore to create a multi-purpose brain template with tissue probability atlases and a corresponding regional atlas for ageing studies. One of the purposes was to use it for regional segmentation of individual older brains, since an old brain template would be a better target for such studies. Another purpose was to use the GM tissue probability map (GM template) to warp the GM regional atlas to other VBM study specific GM templates. This feature was used in **Study II - IV** to warp the atlas to different VBM studies of other study cohorts.

Figure 4.1 shows that the non-linear AGES template of older individuals with mean age 75 years has both more cortical atrophy and larger ventricles compared to the younger ICBM152 template. This demonstrates that older individuals on average differ in brain morphology compared to younger individuals at a large scale.

Older individuals also differ in brain morphology between each other. Especially in ageing, the brain morphology differs quite substantially between individuals, as demonstrated by Sigurdsson et al. (2012). Despite this high brain variability in ageing, the AGES template is still highly detailed and only slightly more blurred than the non-linear ICBM152 template. Figure 4.2 shows a 3D rendering of the template, where the sulci and gyri are highly detailed.

The corresponding regional atlas is shown in Figure 4.3. The results from the validation procedure of the regional atlas showed that 48 out of 56 regions had an average DSC > 0.70. This was regarded as a good score. Regions with a lower score were typically small in size. The Pineal Gland, a very small structure, had a DSC of only 0.23, but all other regions had at least a DSC > 0.60 and the mean DSC across all regions was 0.84. The reproducibility results from the two visits showed better results, where all DSC > 0.70. Also, all regions had an IoI < 0.50, indicating a higher between subject variance than within subject variance. Overall, we considered these results to be robust evidence that the template and regional atlas could be used for regional segmentation in ageing studies.

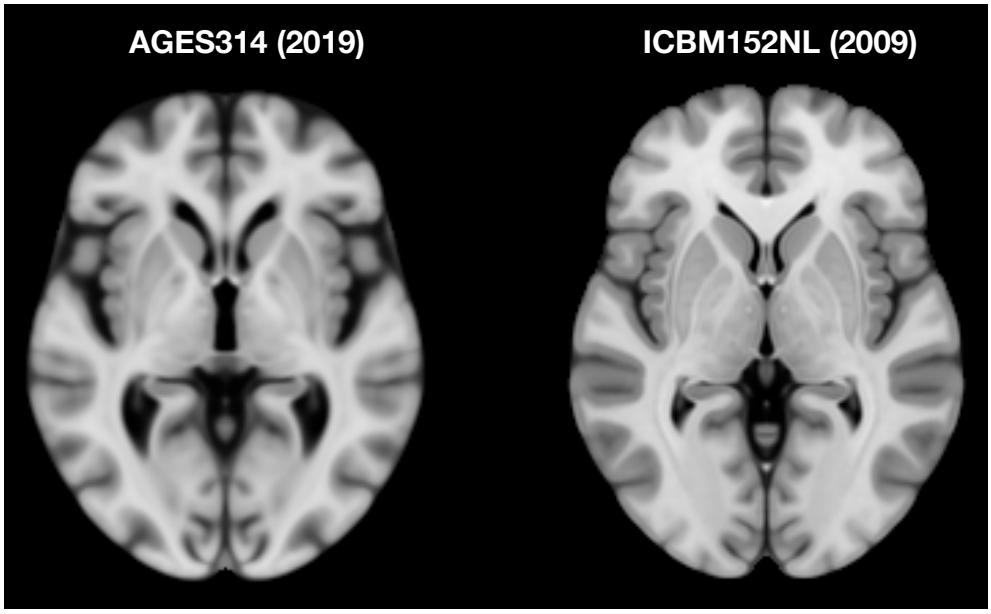

Figure 4.1: On the left side, the non-linear and symmetric AGES template constructed from old individuals with an average age of 75 years. On the right side, the non-linear and symmetric ICBM152 template, constructed from younger individuals with an average age of 25 years. Notable differences are enlarges ventricles and cortical atrophy in the AGES template.

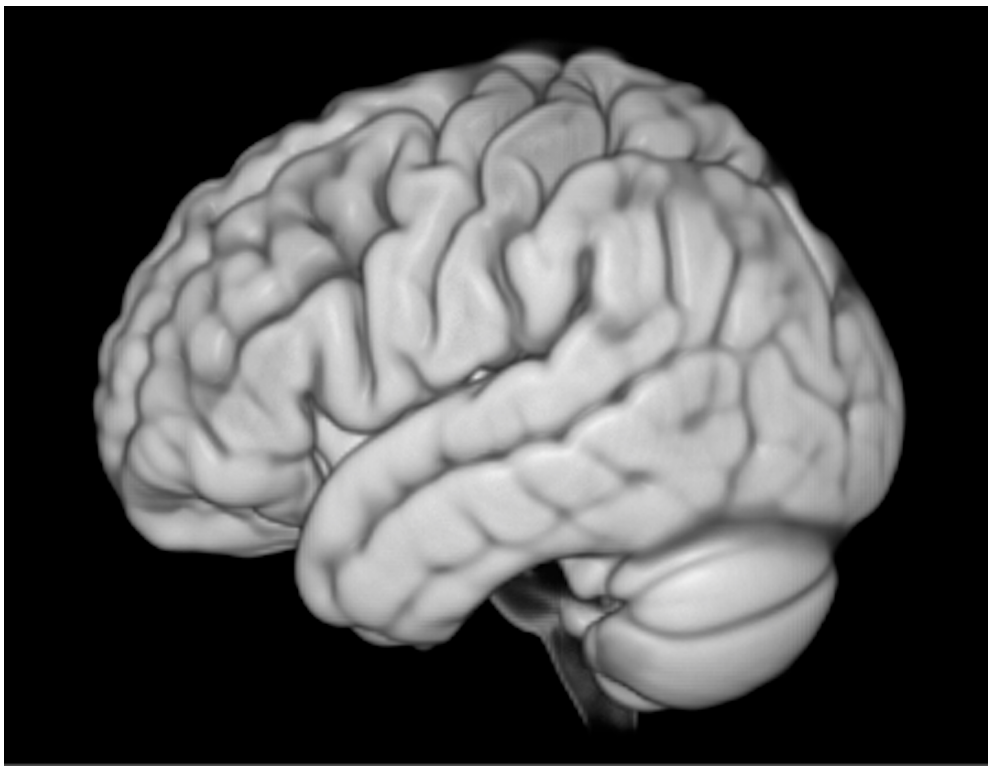

Figure 4.2: The AGES template rendered as a 3D volume. The sulci and gyri of the brain are clearly visible with a high level of detail.

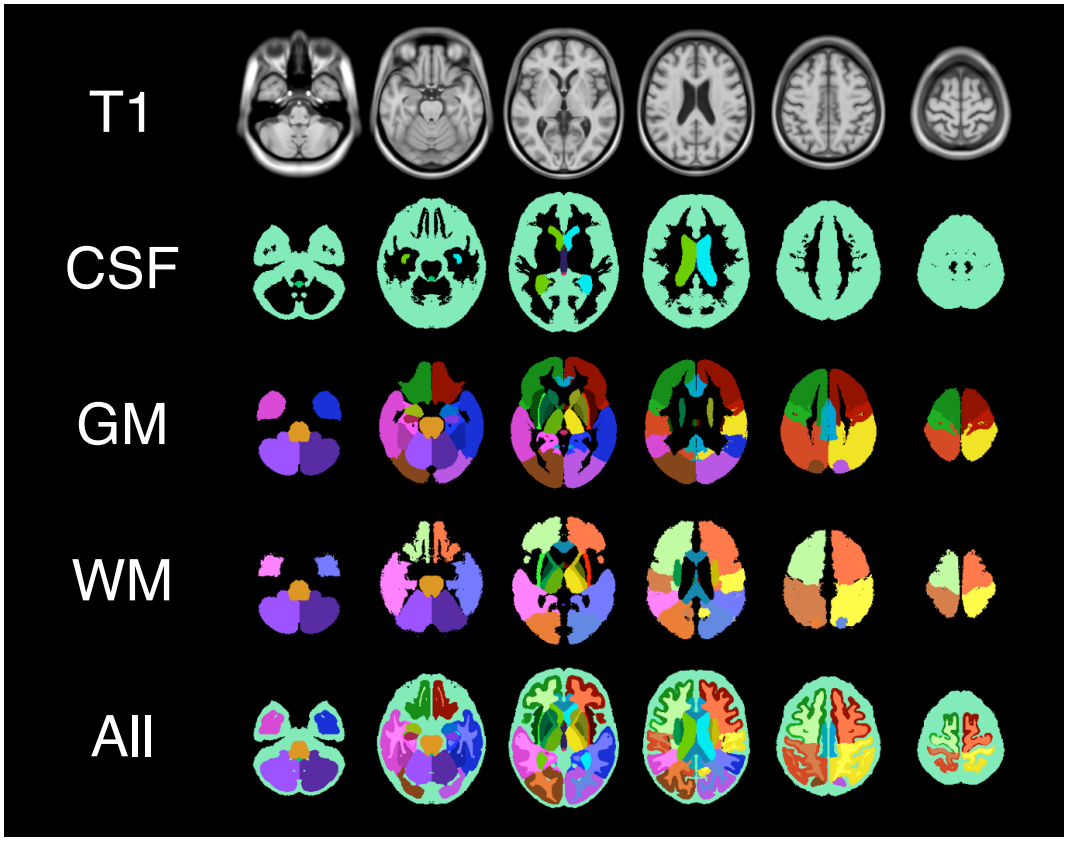

Figure 4.3: The T1-weighted AGES314 template and the different regional tissue atlases along with the combined regional atlas.

4.1.2 Study II

The results from **Study I** lead to an important question. Given that the morphological changes with age are so large that they impact the brain structure at a large scale with enlarged ventricles and cortical atrophy, and given that the ageing process also differ between individuals, we may expect a structural covariability pattern that is driven by the ageing process. How is this variance in brain morphology manifested in old age?

Study II investigated this by looking at which regions in the brain that have a greater level of GM density covariability in the age range 68-83 years. For each GM voxel, we calculated the number of significant correlations in GM density with all the other GM voxels in the brain. Regions with the highest level of covariability were considered as hub regions. These were found in the thalamus, the basal ganglia, the brain stem, and the cerebellum, at the threshold $T = 0.54$ ($p < 0.001$) (Figure 4.4).

However, no significant difference in the covariability pattern could be found between subjects with the age range 68-75 years and the age range 76-83 years (Figure 4.5). Furthermore, a group level covariability map for each age and sex was also constructed to see if there would be any significant change with increasing age or between men and women (32 groups and 30 subjects in each group). Again, no significant difference was found in the covariability levels between the groups. The same covariability pattern emerged in each group. Although we cannot exclude that ageing marginally affects regional covariability level, we found no evidence that the ageing process is the cause of the covariability hubs.

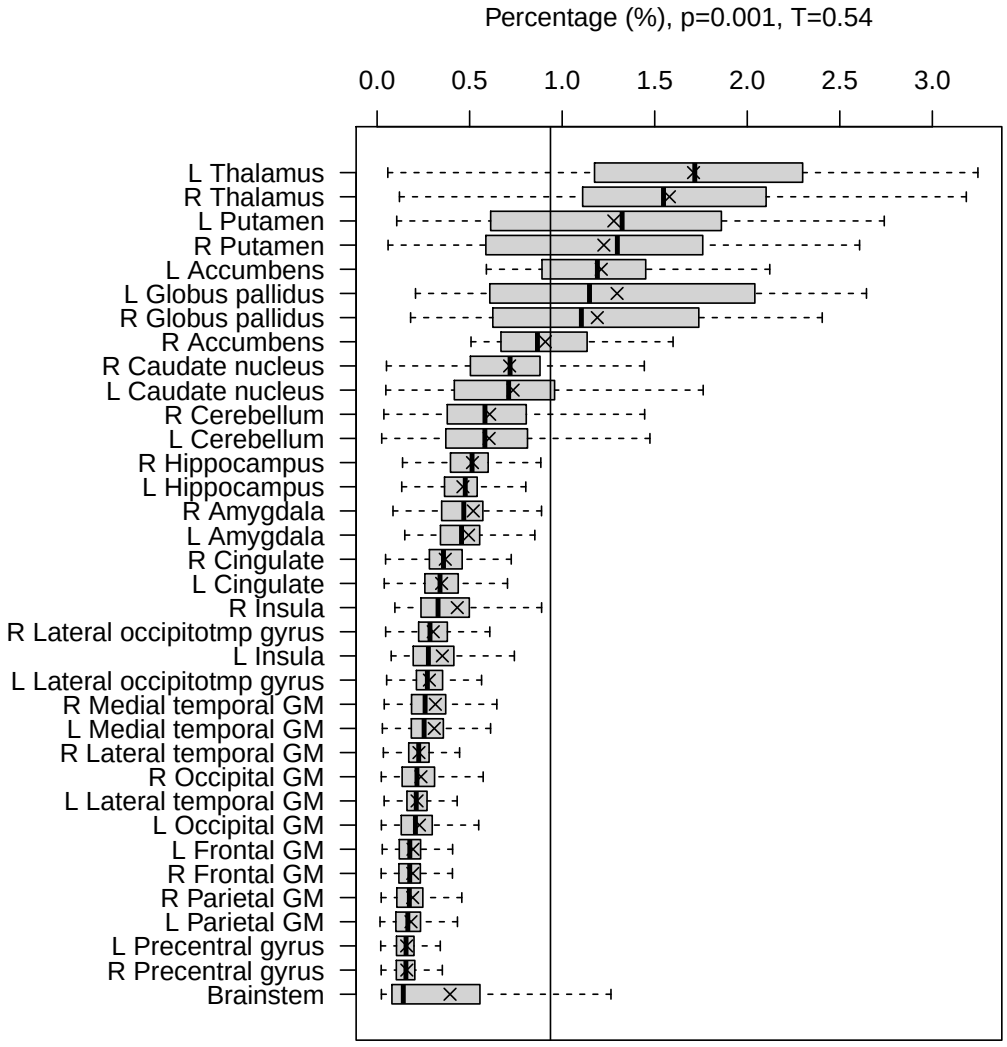

Figure 4.4: Boxplot of the covariability levels in percentage for different regions. The vertical line depicts the covariability level for the top 5% of all voxels with the highest covariability level, which were considered as hubs. These hubs were found in the thalamus, the basal ganglia, the cerebellum, and the brainstem.

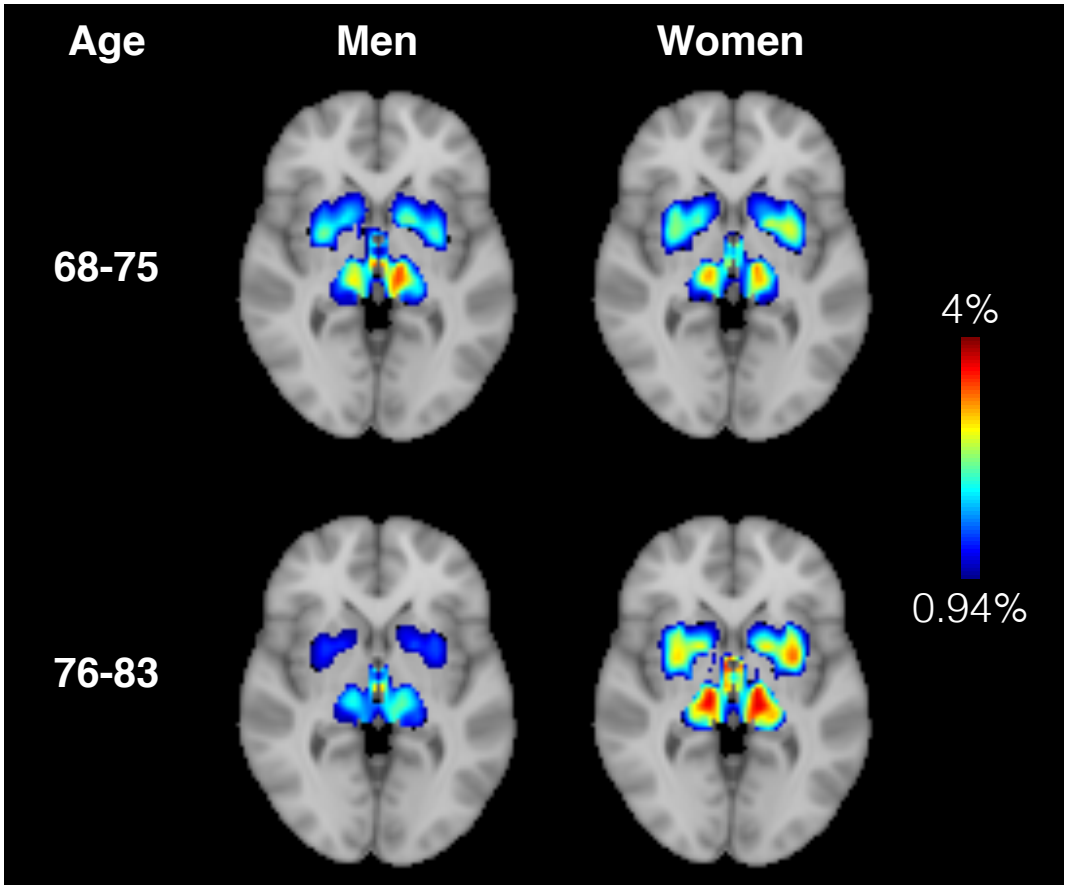

Figure 4.5: The covariability pattern for each of the four groups. No significant difference between the patterns was found. The scale represents the number of significant correlations per voxel in percentage.

4.1.3 Study III

The results in **Study II** indicated a pattern of structural covariability that may not be related to old age. In **Study III**, we therefore investigated if the pattern can be replicated in a population of young adults (age 18-35 years). We also asked if functional connectivity could be a driver for structural covariance. Figure 4.6 demonstrates that the covariability pattern from **Study II** was indeed replicated in a population of young adults, where the thalamus and the basal ganglia were the strongest structural hubs. Figure 4.7 shows a boxplot of the corresponding fGBC levels, with a different order of the functional connectivity hubs compared to the structural covariability hubs.

This study also investigated how much the structural correlation matrix between all GM voxels overlapped with the functional connectivity correlation matrix of the same voxels. The results showed that although there were some overlap, functionally connected voxels did not in general also covary structurally. Figure 4.8 shows the boxplot of the intersection between structural covariance and functional connectivity, and Figure 4.9 shows the comparison between the structural covariability map, the fGBC map, and their overlap.

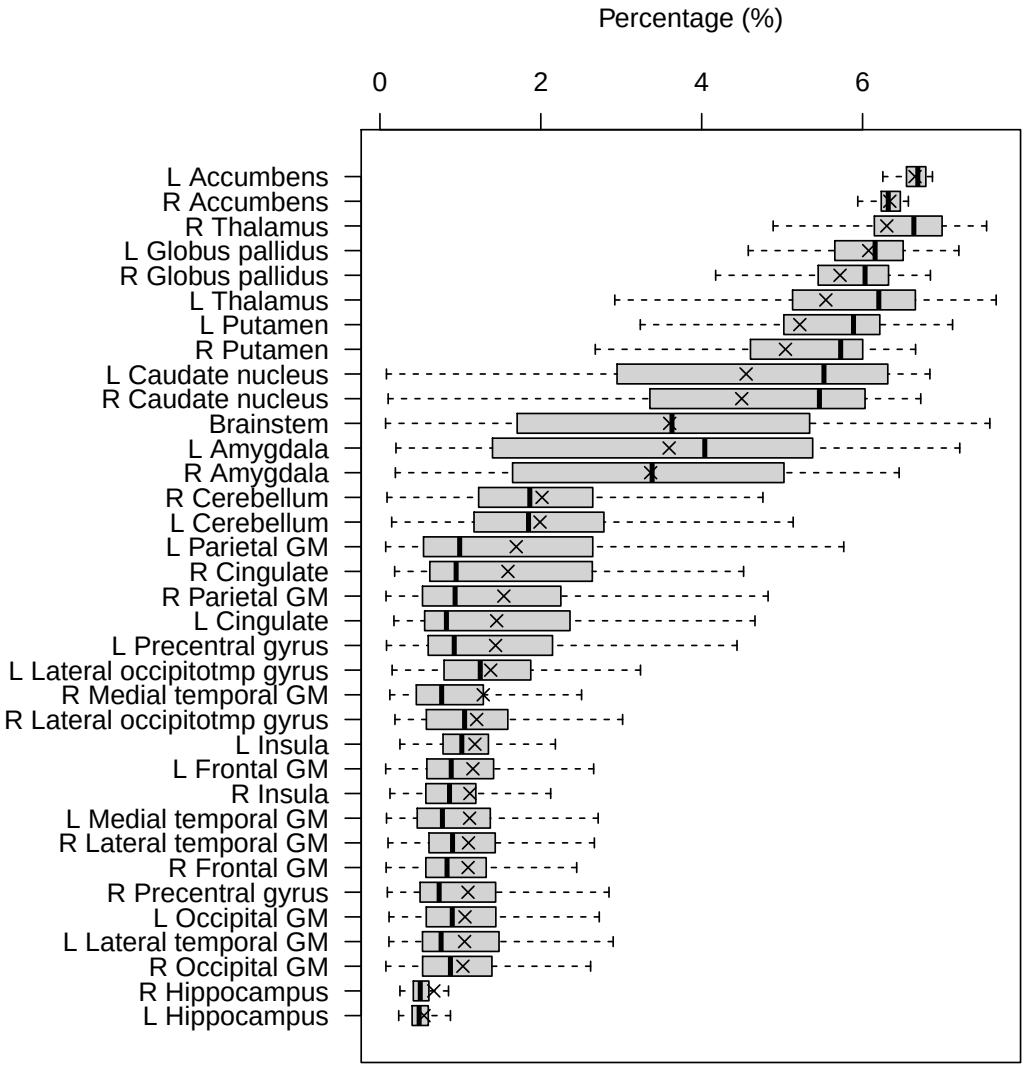

Figure 4.6: Boxplot of the covariability levels in percentage for different regions in a cohort of young adults. The order of the regions is similar to **Study I**, with the thalamus and the basal ganglia having the highest level of covariability.

One hypothesis for the existence of covariability hubs in old people could be that the ageing related variability in ventricle size of older people would affect neighbouring regions and therefore give rise to the covariability. However, since the same results emerged in young adults, the conclusion is that age cannot be the driving factor of these covariability hubs and that the covariability hubs between young adults are well preserved to old age.

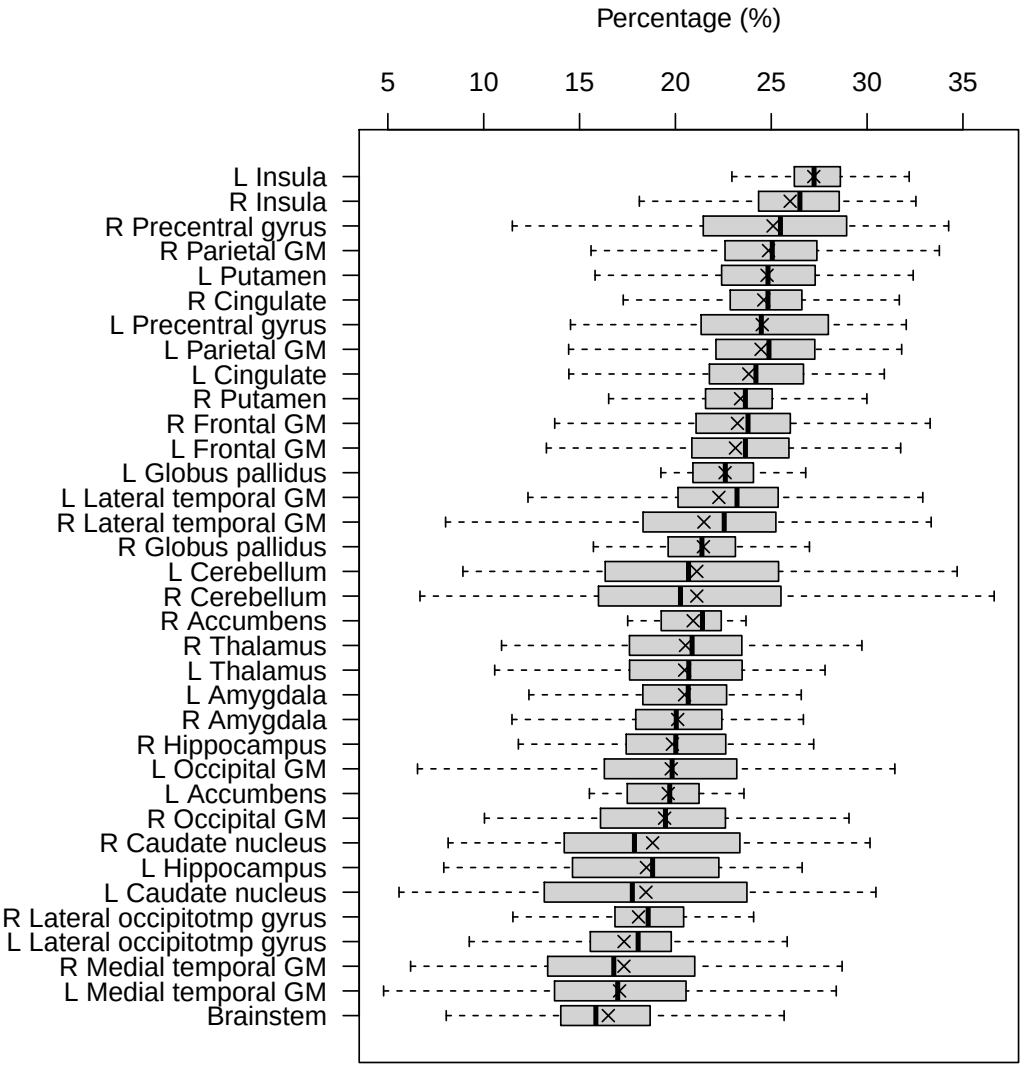

Figure 4.7: Boxplot of the functional global brain connectivity levels in percentage for different regions in a cohort of young adults. The order is very different from the covarability results.

Another hypothesis for these hubs is that an underlying functional connectivity could give rise to structural covariance. Two functionally connected regions may due to neuroplastic mechanisms form more synaptic connections, resulting in increased GM density. If the within-individual functional connectivity also vary between individuals, this may lead to a corresponding structural covariance between individuals. Some overlap between the two matrices were indeed found in the subcortical regions. However, if this was a general principle, one could expect a quite large overlap between the functional connectivity and the structural covariance for all voxel pairs, which was not the case.

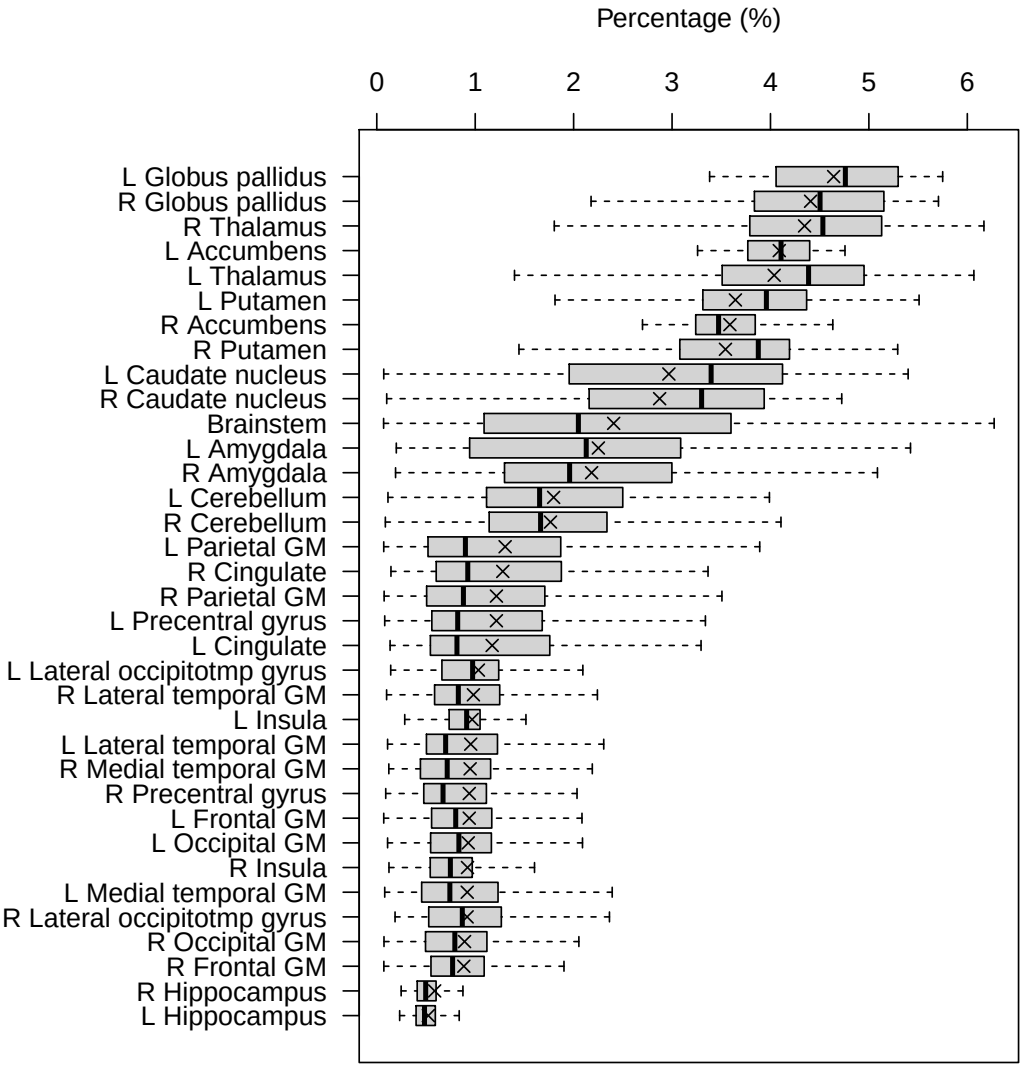

Figure 4.8: Boxplot of the overlapping functional connectivity and structural covariance for each region. Most of the overlap is found in the subcortical covariability hubs.

4.1.4 Study IV

In **Study IV**, we first investigated if there were any differences in the covariability levels for GM density maps and GM volume maps. The result showed that the same regions appeared as covariability hubs (Figure 4.10). However, GM volume maps resulted in a slightly higher covariability level for all regions and were therefore used for the rest of the study because they did not reduce the inter-subject variance.

In order to further understand the principles of how these subcortical regions become hub regions, **Study IV** used a variational autoencoder that could reproduce the hubs in a dimensionally reduced latent space. The results showed that only four dimensions (or factors) were required to reproduce the majority of all significant correlations (Figure 4.11 and 4.12).

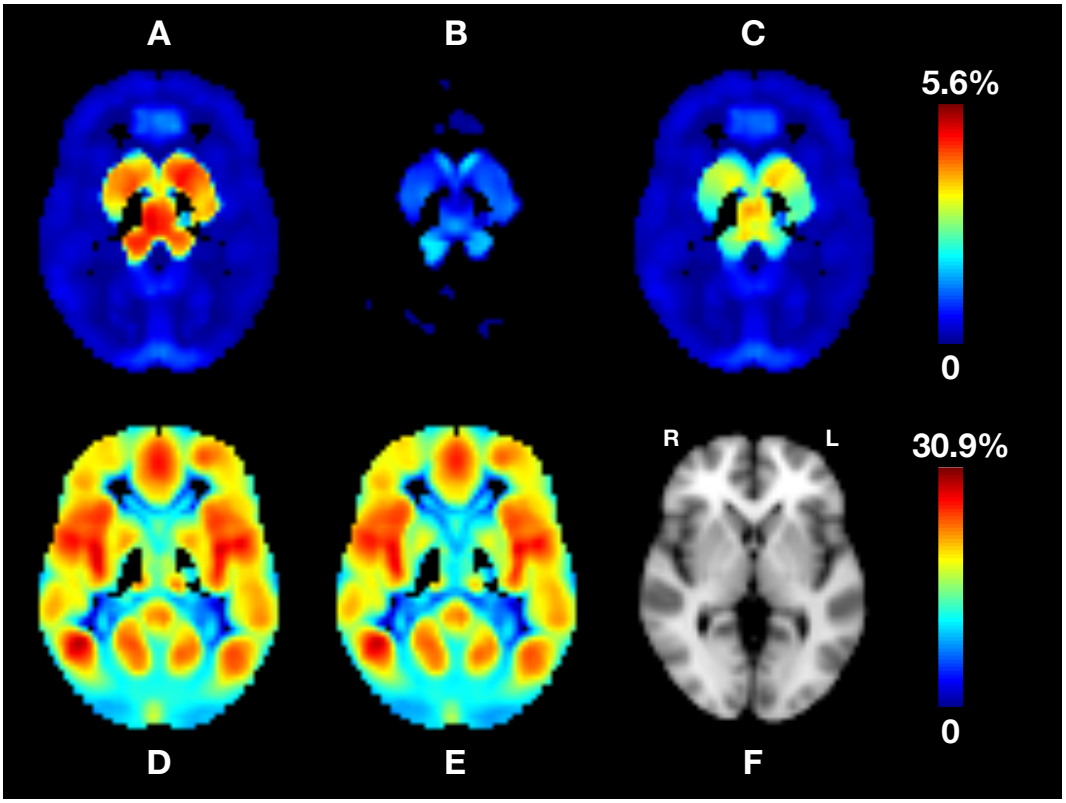

Figure 4.9: A: The structural covariability map. B: The structural covariability map that do not overlap with functional connectivity. C: The structral covariability map that overlap with functional connectivity. D: Global functional connectivity map, where many regions have a high level of significant functional connectivity. E: Global function connectivity map between voxels having no underlying significant structural correlation. F: The MNI template. The scale represents the number of significant correlations per voxel in percentage.

When using the latent factors as explanatory variables in a VBM analysis, the results showed that subcortical regions had a tendency to always covary across the entire latent space as long as there were an underlying variance in these regions. The first factor correlated positively with all GM regions. The second factor correlated with both subcortical regions and fronto-parietal GM regions. The third factor correlated with cortical regions but not subcortical regions. This lack of variation in factor 3 were consistent across the subcortical regions. The fourth factor had an interesting pattern of both positive correlations with subcortical regions and negative correlations with cortical regions (Figure 4.13).

Other regions, such as the cingulate and the insula, were not consistent in their correlations with other regions. For factors 1 and 2, the cingulate had a positive correlation with the subcortical hubs. For factor 4, the correlation was negative. Hence, it did not maintain a high covariability across the entire latent space. By reducing the variance of the first factor, we could study how this would change the covariability levels.

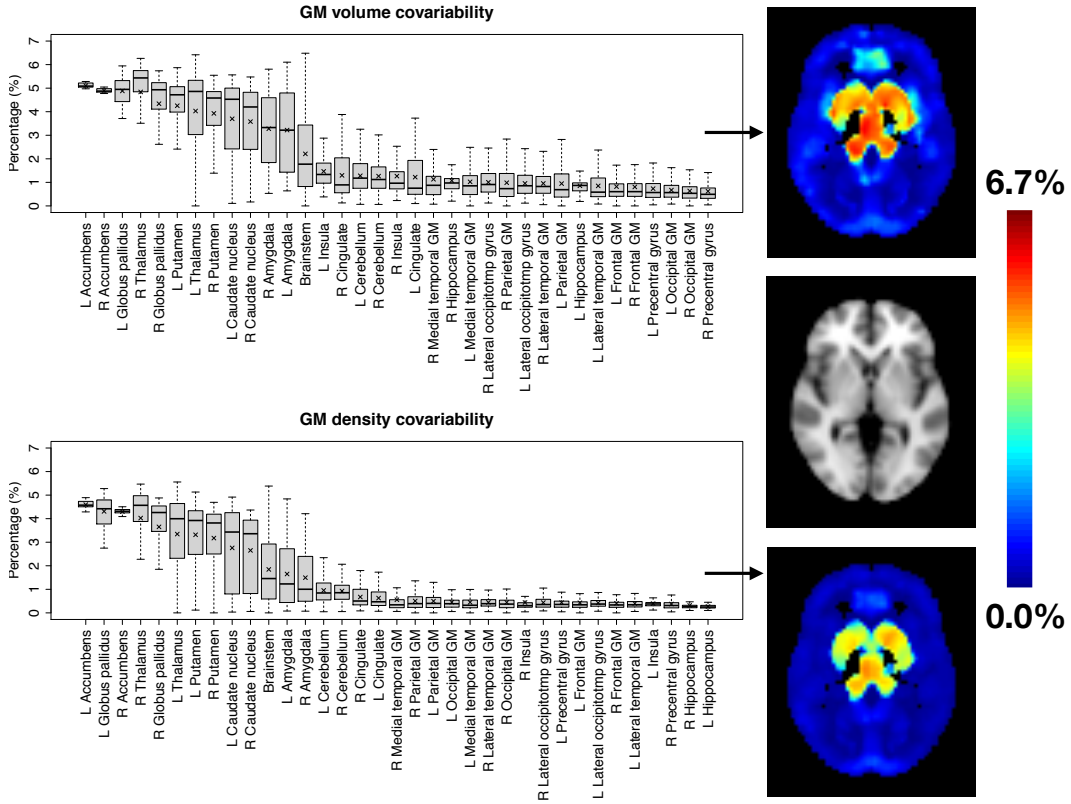

Figure 4.10: The difference in covariability level between GM volume and GM density maps within each GM region. The hub regions remained the same, with the thalamus and the basal ganglia as the regions with the highest covariability levels. The GM volume maps resulted in a slightly higher covariability pattern overall.

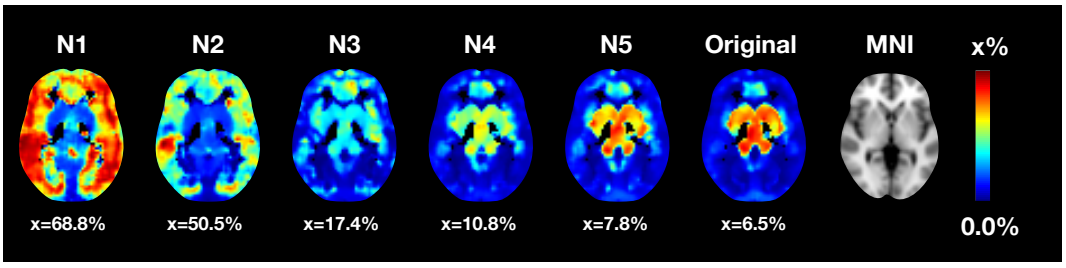

Figure 4.11: The results from reconstructing the covariability pattern using autoencoders with different number of latent factors. The structural covariability hubs start to appear already in network N3 (with 3 latent factors), but 4 latent factors are needed to reconstruct a majority of all significant correlations as shown by network N4. The scale represents the number of significant correlations per voxel in percentage.

This was done by selecting the 69 subjects with the lowest variance in factor 1. A random set of 69 individuals was also selected as comparison. The results showed a quite different order of the regions for the limited variance subset, with the insula, the cingulate, and frontal GM having the highest level of covariability, while the subcortical hubs only increased slightly in the covariability level (Figure 4.14).

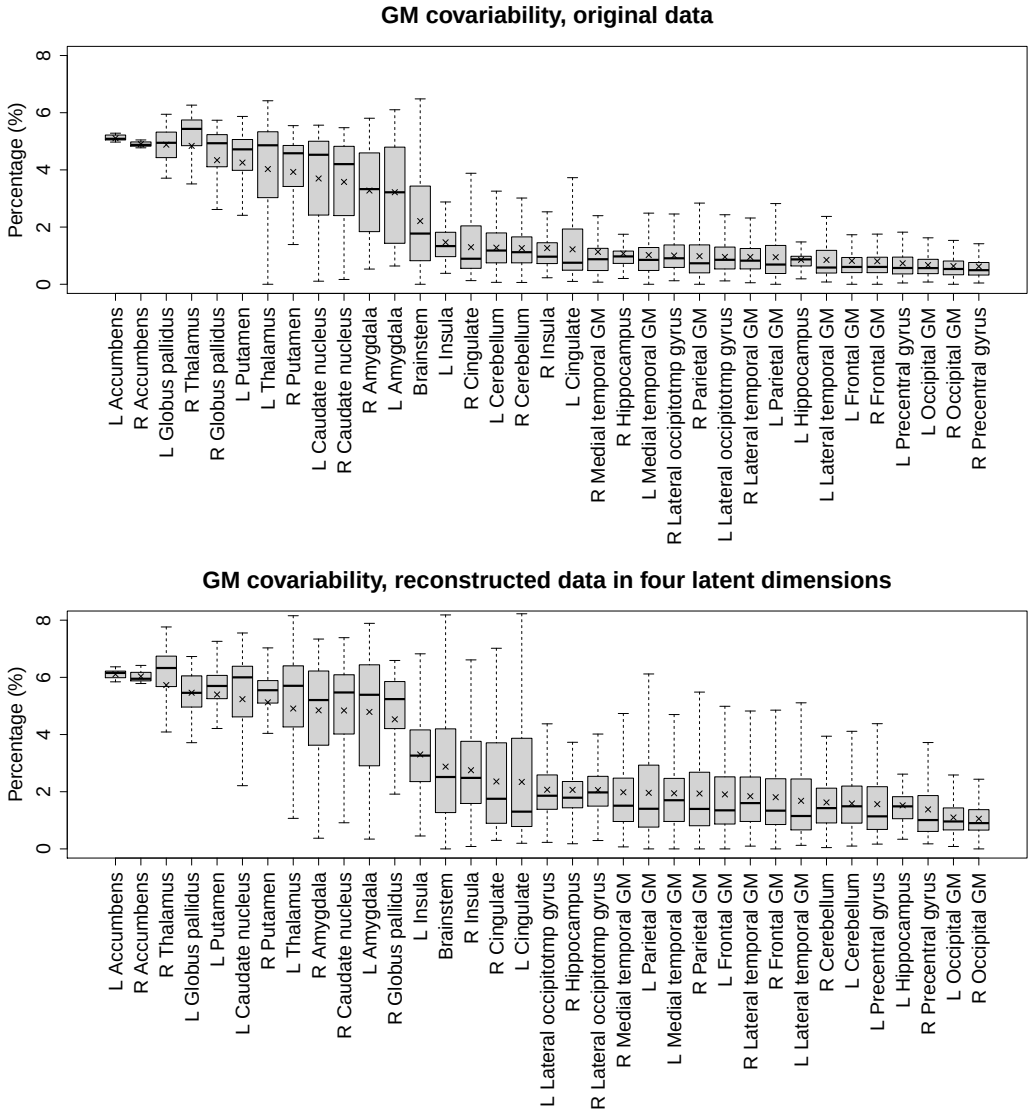

Figure 4.12: A boxplot of the covariability levels for the original data compared to a boxplot of the reconstructed data at four latent dimensions.

The four factors also correlated with other phenotypic variables. Factor 1 and 3 correlated significantly with total GM volume, and factor 3 correlated significantly also with total GM density. Factor 4 had a significant negative correlation with both age and total GM volume. Although FIQ correlated significantly with total GM volume, even from the reconstructed data, it did not correlate significantly with any specific factors. The result from the correlation with fGBC, also shown in Figure 4.13, showed that factors with a positive subcortical correlation in the VBM also correlated with a widespread cortical increase in functional connectivity.

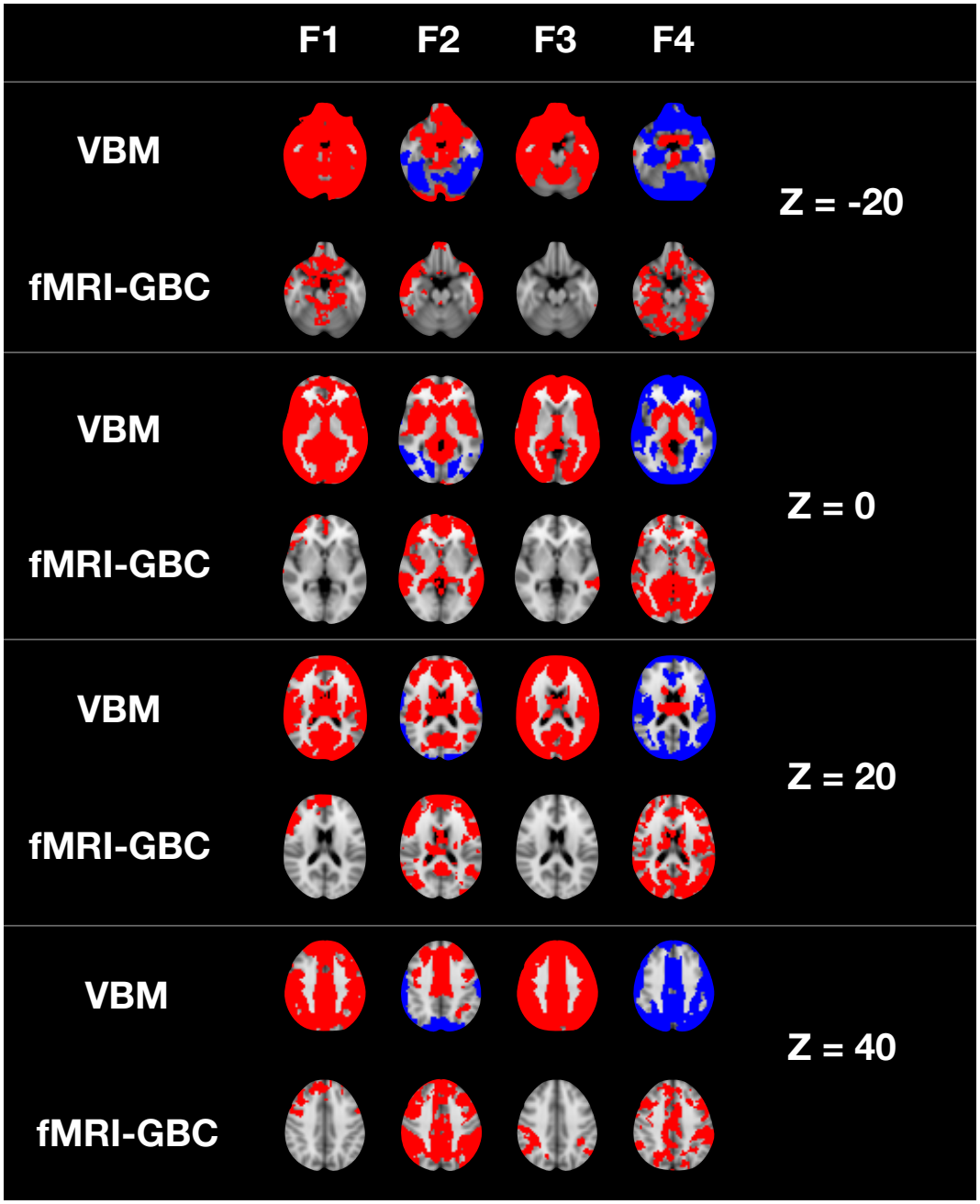

Figure 4.13: VBM and fGBC GLM analyses, with latent factors from the autoencoder N4 as regressors. Red colour represents positive correlations and blue colour represents negative correlations.

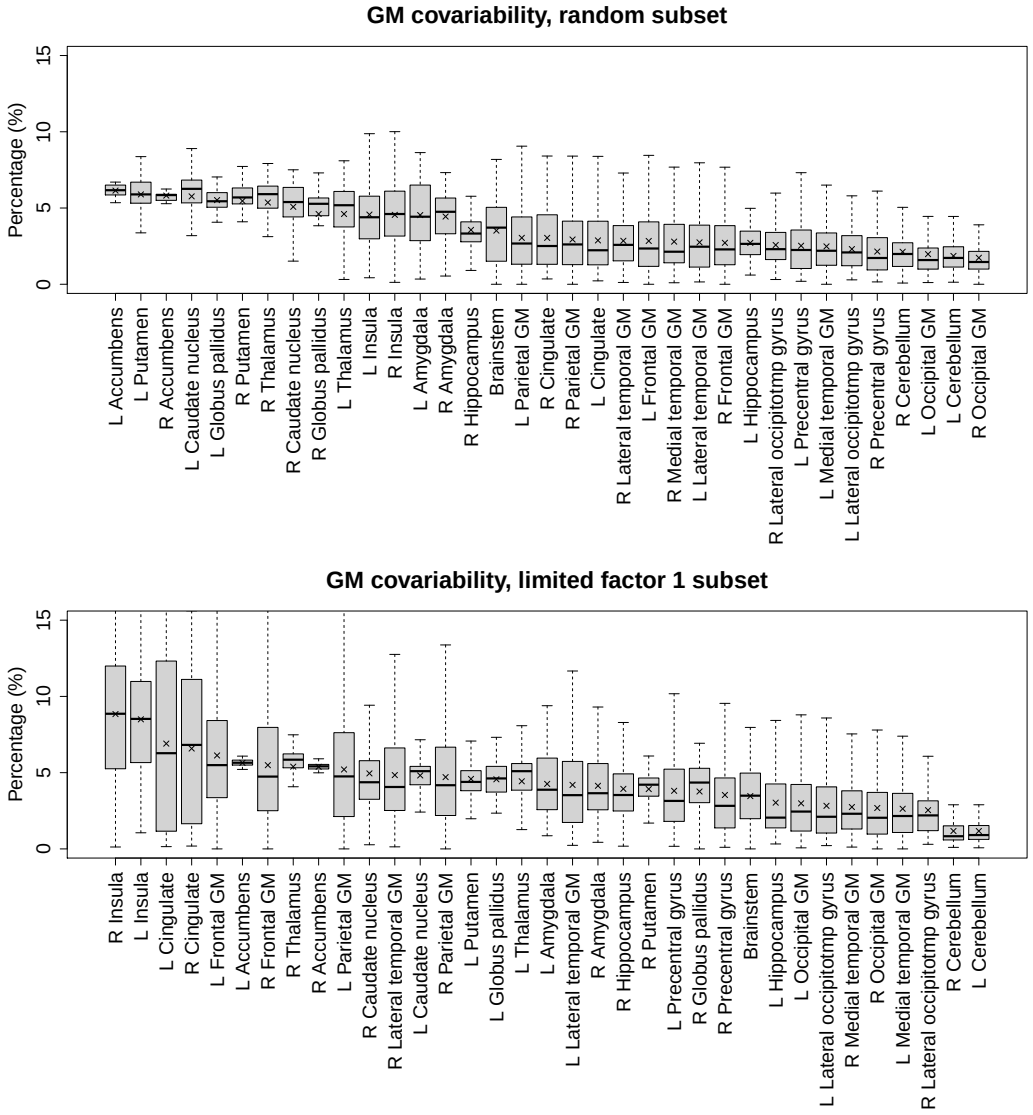

Figure 4.14: A boxplot demonstrating the covariability levels of a random subset of 69 individuals (top) and a latent space of 69 individuals where the variance in factor 1 was reduced. The results showed that the covariability of the insula, the cingulate, and the frontal GM, got a higher level of covariability in the reduced latent space.

4.2 Sources of structural covariance

The causes of structural covariance have previously been discussed in other studies. One conclusion is that both genetical and environmental factors are likely to be involved and that the covariance may be in part related to differences in individual behaviour (Mechelli et al., 2005). It is indeed an interesting observation that some of the hubs were found within the basal ganglia, which consists of subcortical structures involved in many different behaviours (Arsalidou et al., 2013). These structures are also highly interconnected with the cerebral cortex.

One interesting thing to note in that respect is that the latent factors in **Study IV** that correlated positively with the volume in basal ganglia regions also correlated positively with increasing functional connectivity in cortical regions. In other words, individuals with increased basal ganglia volume also tend to have an overall increased functional connectivity throughout the cerebral cortex.

Studies have shown that common genetic variants may explain up to 80% of the variance in regional brain volume (Zhao et al., 2019). This connection has also been observed in the thalamus (Elvsåshagen et al., 2021) and the basal ganglia (Bryant et al., 2013), indicating that genetic factors may play an important role for the subcortical hubs. One study explored in particular the genetic covariation with volumes of subcortical regions and found four distinct genetic factors: a basal ganglia/thalamus factor, a separate nucleus accumbens factor, a ventricular factor, and a limbic factor (Eyler et al., 2011).

Other factors that have been discussed as sources of structural covariance are mutual trophic influences, experience-related plasticity, and normal development and ageing (Evans, 2013). There are indeed evidence of an activity-dependent plasticity for certain types of learning in the basal ganglia (Wickens, 2009). However, as we have seen in this thesis, ageing seems not to be a major factor behind the subcortical hubs since these hubs appear throughout the age span.

4.3 Comparison to other studies

The brain template of older individuals from **Study I** resembles that of other templates at old age (Fillmore et al., 2015; Dadar et al., 2022), with very similar characteristics of cortical atrophy and enhanced ventricles compared to the young adult MNI template. However, the aim of the AGES atlases was not only to create a brain template but also a corresponding regional atlas and tissue atlases (including WM lesions), to allow it to be used for multiple purposes including warping the regional atlas to other study cohorts by using the GM tissue probability map. As far as we know, this makes the AGES atlas still unique.

Study II - IV are the first studies we know of to investigate large scale structural covariance across the entire brain using all voxels as seeds. Other studies have either used seed voxel analyses of a few voxels, graph theoretical approaches at a regional level, or ICA on GM (Mechelli et al., 2005; Xu et al., 2009; Evans, 2013; Smith et al., 2019). Hence, a direct comparison is difficult to obtain. Some covariance studies are based on cortical thickness, where two studies found hubs in the association cortices (He et al., 2007; Chen et al., 2008). Being based on cortical thickness methodology, these studies excluded subcortical structure in the analysis so the results are difficult to compare with a VBM approach.

Nevertheless, the absence of an age-related change in covariability at old age in **Study II** is consistent with a few other studies. One study used graph theory to compare local efficiency between three different age groups. The result showed differences between the young group and the middle aged group, but no differences between a middle aged group and an old group of subjects (Wu et al., 2012). Another study found the structural covariance patterns to be relatively stable at old age but that the pattern changed from younger to middle age (DuPre and Spreng, 2017). The results in this thesis do not exclude that the subcortical hubs are influenced by ageing processes to some degree. What is demonstrated is that they exist as hubs independent of age.

Another study used ICA on VBM GM maps and identified the precuneus, the fusiform area, the posterior intraparietal sulcus, and the dorsolateral prefrontal cortex to be the most common GM regions across the independent components maps, without any indications of the thalamus and the basal ganglia in the maps (Smith et al., 2019). However, a similar ICA on VBM study found the thalamus and the basal ganglia as two separated independent components maps (Xu et al., 2009). Also, patterns of structural covariance have been identified in the basal ganglia based on four seeds in the neostriatum (Soriano-Mas et al., 2013).

Some studies have investigated a potential relationship between functional connectivity and structural covariance. One study looked specifically at nine different seed voxels in the default mode network, task positive network, and sensory networks, and found similar patterns between functional connectivity and structural covariance for some of the seeds (Zhang et al., 2011). Another study used ICA for both structural covariance and functional connectivity and found independent component maps that were similar between the two modalities (Smith et al., 2019). However, a third study only found a limited relationship based on nine seed regions (Reid et al., 2017).

In **Study III**, we did not find that functional connectivity would give rise to structural covariance as a general principle. However, some overlap between structural covariance and functional connectivity in the subcortical hubs were found. This seems also to be in line with the study by Soriano-Mas et al. (2013), who found that neostriatal structural covariance patterns overlapped well with the corresponding functional connectivity networks, and the study by Segall et al. (2012) who identified the basal ganglia structures to have the strongest structural to functional correlation using ICA.

In **Study IV**, we found four latent factors that correlated well with different aspects of GM and that could replicate a majority of the significant structural correlations. One of the factors (F4) correlated with a distinct pattern of voxels in the subcortical regions (see Figure 4.13). The variational autoencoder provides a non-linear component analysis similar to other studies using non-linear component analysis. In one of these studies, they found distinct non-linear patterns in the basal ganglia and the thalamus that were different between schizophrenia patients and controls (Castro et al., 2016).

4.4 Evolutionary perspectives

The subcortical hubs are evolutionary old regions that have been preserved through vertebrate evolution, where the basal ganglia are thought to have evolved over 560 million years ago (Stephenson-Jones et al., 2011; Grillner and Robertson, 2016) and belong to an ensemble of highly connected regions involved in higher-order behaviours together with the thalamus (Bell and Shine, 2016).

The basal ganglia appeared in vertebrate evolution at the time of the Cambrian explosion, which filled the seas with a vast diversity of animals. The Cambrian explosion is seen as the most significant event in evolution, which possibly emerged from a complex interplay of environmental changes including a sudden rise in oxygen that may have enabled the emergence of carnivores and predators (Fox, 2016).

Being a system for selection of behaviour, motor learning and value-based decisions, the basal ganglia were possibly at the very core of this leap in evolution. It had to evolve rapidly to incorporate new behaviours necessary for survival in an ever-changing competitive environment. Grillner and Robertson (2016) noted that the number of modules in the basal ganglia had to increase progressively during vertebrate evolution. However, evolving new functionality solely through mutation is expensive and takes time. A faster process would be to evolve new modules with a similar design as the older modules to control new behaviours. This process, where an ancestral core is reused for new functions, is known as exaptation (Grillner and Robertson, 2016).

It has been shown that the basal ganglia of the lamprey has all the parts of the mammalian basal ganglia, but with simpler circuits, demonstrating that the basal ganglia circuitry has been conserved, reused, and expanded through evolution (Stephenson-Jones et al., 2011). Rather than generating new structures, it is quicker to reuse and extend existing networks. As an example, the structures of the cortico-basal ganglia-thalamo-cortical loop, with its direct pathway to initiate and execute voluntary movement and indirect pathway to inhibit behaviour, do exist in the lamprey but consist of a much more complex network in the human brain (Grillner and Robertson, 2016; Parent and Hazrati, 1995).

Another evolutionary process that will lead to faster evolution is to reutilise already existing genetic variants from its ancestors. This inheritance is called standing genetic variation and the evolvability of a population depends highly on it (Barrett and Schluter, 2008; Lai et al., 2019). A standing genetic variation through evolution will eventually lead to a genetic variability that is shared across species (phylogenetic variability) as the branches in the pylogenetic tree are splitting. As a result, the variation in structure seen in the human brain resembles that of other species, probably due to phylogenetic variability (Charvet et al., 2013).

These two evolutionary processes are probably at interplay. The standing genetic variation allows to inherit and store different genetic variants across the species DNA, which could potentially cause GM volume variance in the subcortical regions. Studies have indeed demonstrated a genetic correlation with both the thalamus and the basal ganglia (Elvsåshagen et al., 2021; Bryant et al., 2013). At the same time, the exaptation process have created intricate networks in the subcortical regions through evolution that evidently also covary structurally across individuals.

Combined, these two processes may lead to inter-individual variance in both functional connectivity and structural covariance. In **Study IV**, there were evidence that some latent factors would correlate with both subcortical brain volume and inter-individual increase in fGBC (see Figure 4.13). In **Study III**, there were also some evidence of a shared within-individual functional connectivity and inter-individual covariance in the subcortical hub regions (see Figure 4.9).

At the same time, on individual level, adaptation to a new environment has to be done at a synaptic plasticity level for survival and several parts of the basal ganglia are also susceptible to synaptic plasticity (Wickens, 2009). If both genetic and environmental factors are causing variance in subcortical volume, it is plausible that these factors would be embedded in the latent space from **Study IV**. The subcortical regions maintained a high covariability level throughout the entire latent space. Thus, it may be that these subcortical hubs origins from both genetic and environmental factors.

5 Conclusions, limitations and future perspectives

5.1 Conclusion

The main aim of this thesis has been to understand the principles of structural brain variance that cause different brains to have different shape and size. The development of a standard template of old individuals (mean age 75) showed cortical atrophy and increased ventricles compared to the MNI template of younger individuals (**Study I**). From this, we can conclude that ageing is one important factor for morphological differences between individuals.

However, when studying which voxels that have the highest level of covariability, the results showed that voxels in the subcortical regions, the thalamus and the basal ganglia, had the highest covariability both for individuals at old age (68-83 years, **Study II**) and younger age (18-35 years, **Study III & IV**). By using a variation autoencoder to obtain a dimensionally reduced latent space (**Study IV**), we found that the correlations between the structures in these subcortical hubs are maintained as we span across the whole latent space. This is not true for other structures such as the frontal lobe, which obtained a higher covariability when the latent space was reduced. If the latent space contains both environmental and genetic factors that correlate with subcortical structures, a conclusion could be that the correlations between the subcortical regions are similar across the different factors.

An interesting connection between increased basal ganglia volume and an overall increase in cortical fGBC was found for some factors, indicating that there is a relationship between structural covariance and functional connectivity (**Study IV**). However, we found no indication that the functional connection between two voxels would commonly give rise to an inter-individual structural covariance between the same two voxels (**Study III**). Most voxel pairs did not have both a functional connection and a structural covariance.

5.2 Limitations and future perspectives

These studies have a number of limitations that need to be addressed. In **Study I**, the number of subjects used to create the regional atlas was limited to four subjects and only three subjects were used for validation. However, the AGES template itself was created from 314 subjects. One approach could have been to label the actual AGES template instead of individual subjects, but we found it easier to locate certain borders within the individual subjects and then warp the results to the template. More validation subjects would be necessary to draw larger conclusions. Nevertheless, the manual inspection of the final results demonstrated a regional atlas with quite accurate delineations between regions.

In **Study II**, the regional atlas was used to define the level of covariability in each region. The age range of the study cohort was similar to the AGES template and by obtaining the deformation field between the AGES GM probability map and the study specific GM probability map obtained from the VBM study, it was possible to warp the atlas to the VBM study space. However, in **Study III** and **Study IV**, the study cohort is between 18 to 35 years. The rationale for using the same procedure here, was that we needed the same definitions of the regions to be able to compare the results. A visual inspection of the AGES atlas after warping to the VBM template showed that it was accurate enough for the purpose of the study, reflected also by the results.

This work has hypothesised that both environmental and genetic factors have influenced the structural covariability levels. However, we do not know how the latent factors map to these external factors. If the genetic variance could be separated from the environmental variance, it should be possible to compute a covariability map that only represents environmental factors and another covariability map representing only genetic factors. In principle, this could be done using large genetically informative data sets, e.g. from twins. Once separated, the latent space of the variational autencoder could also be mapped based on this information.

The difference between an autoencoder and a variational autoencoder is that the latter is a so called generative model. It can generate new samples of simulated brain images by sampling points in the variational space from which it has not been trained. This is done by learning the probability distribution of the input data. We did not have enough subjects to train and validate the network for this purpose.

However, with more subjects, it may be possible to create a latent space of the structural covariances where the morphology of simulated brains could be studied and the latent space could be clustered into different features. Another interesting aspect is to investigate how individuals with a neurodegenerative disease would move through the latent space as the disease is progressing. This could give further insights into the mechanisms of the disease and could potentially also be used as a prediction tool based on the trajectories of other individuals.

6 Acknowledgements

This last chapter concludes a long journey. There are many friends and colleagues along this journey who have influenced and contributed with support throughout the years, to whom I hold my deepest gratitude. A huge thanks to you all and my sincere apologies to anyone I missed! My gratitudes go:

To **Fredrik Ullén**, my main supervisor for the most part of my doctoral studies. We met many years ago with a common interest in looking at brain variability in a large cohort. This thesis represents the outcome of that interest. Thank you for staying with me and never giving up on me throughout these years. Thanks you also for the academic freedom you have given me in making this work a reality. You embraced my ideas and then guided me forward to make them true. Finally, thank you also for all the interesting discussions we had about everything from evolution, music, butterflies, and Z80 processors.

To **Per Roland**, my first main supervisor, for taking me on as your doctoral student and for the academic freedom you gave me. You always supported me and my ideas in the early work we did together, even before my doctoral studies.

To **Vilmundur Guðnason**, my co-supervisor in Iceland. You embraced the idea of making a PhD out of my work at the Icelandic Heart Association and supported my ideas. Thanks for all your wise words, including the one to follow the direction where my heart lies. I did and here I am.

To **Gert Svensson**, my previous manager at the PDC Center for High Performance Computing, for being the person who initially pushed me into the neuroimaging research field and for supporting me and giving me the freedom to explore new ideas during the early years.

To all the colleagues and former colleagues at Fredrik Ulléns research group, **Karen Kuckelkorn**, **Laura Babcock**, and **Miriam Mosing**, for all the interesting discussions we had at the lab. A special thanks to **Örjan de Manzano** for supporting and co-authoring my final two manuscripts.

To previous colleagues and related collaborators at Per Roland's research group, **Michael Harvey**, **David Eriksson**, **Carl Undeman**, **Jeremy Young**, **Stylianos Papaioannou**, and **Malgorzata Gut** from Nencki Institute of Experimental Biology, for all the great work and all the great discussions we had during my early years in brain research.

To all my previous colleagues at the Icelandic Heart Assocation and associated collaborators, **Bryndis Oskarsdottir**, **Asdis Egilsdottir**, **Olafur Kjartansson**, **Hjörleifur Halldorsson**, **Fjóla Jóhannesdóttir**, **Thor Aspelund**, **Mark van Buchem** from Leiden University, **Laura de Jong** from Leiden University, and **Lenore Launer** from National Institutes of Health. Especially a big thanks to **Sigurður Sigurðsson** for all the support and to **Alex Zijdenbos** from Biospective, my senior author of my first paper. I have learned so much about neuroimaging from both of you.

To all my previous colleagues at Raförninn, including my previous co-supervisor, manager, and mentor **Smári Kristinsson** for supporting my decision to become a doctoral student as part of our work.

To **Niklas Ljung**, **Håkan Dahlbom**, and **Gunnar Stjernberg** at Synective, to **Jonas Åström** at Intel, and to **Nikolay Rognlien** at Arrow, for your efforts in helping me learn more about using FPGA and OpenCL in brain science.

To all my new colleagues at Jan Hillert's research group and at the Swedish MS registry, including **Pernilla Klyve**, **Tim Spelman**, **Athanasia Christakou**, **Elena Mouresan**, **Anna He**, **Anna Cunningham**, **Eva-Carin Jacobsson**, **Lillemor Bergström**, **Ryan Ramanujam**, **Ali Manouchehrinia**, **Kyla McKay**, **Virginija Karrenbauer**, **Sahl Bedri**, **Katharina Fink**, and **Anna Hedström**. A special thanks to **Jan Hillert** for being my mentor and supporting my work, **Anna Glaser** for always having the time for questions and discussions, and **Leszek Stawiarz** for all the interesting brain discussions we had regarding atrophy and neurodegenerative processes.

To **Sophie Okane** and **Konstantina Kilteni** from the cognition corridor, for always being so nice, friendly and supportive.

To **Eva Noréns** from the administration at the Department of Neuroscience, for all the encouragements and support.

To my neighbours, **Birgitta Wretling** and **Anders Wretling**, for being the best neighbours in the world and for your encouragements.

To **Fredrik Feurst**, for all the advices you gave me on deep learning for my final manuscript.

To **Lucas Forsberg** and **Tyra Midbrink**, who plan to perform at the dissertation dinner, and to **Sandra Löfgren** for offering them extra trombone lessons for this event.

To my friends, with families, **Henrik Ehrsson**, **Jesper Fredriksson**, **Jonas Käll**, **Peter Marklund**, and **Anders Arpteg**, for all the encouragements, interesting discussions, dinners, and trips we have done together.

To my childhood friend, **Marcus Modin**, for our life long friendship, support and care, and to his partner **Linda Sandström**, and their sons **Liam Modin** and **Olle Modin**, for all the fun and joyful times our families have together.

To my friends **Lisa Midbrink** and **David Andersson**, and their daughters **Tyra Midbrink** and **Alva Midbrink**, for all the encouragements, fun and interesting discussions our families have together.

To my friends, **Katarina Nordling** and **Lars Nordling**, and their daughters **Ida Nordling** and **Greta Nordling**, for all your encouragements and for all the boat adventures our families have together.

To my relatives, **Jannice Gårdh** and **Roland Gårdh**, for your love and care. You have always been an inspiring source for me and I know you are always a phone call away when I need you.

To my parents-in-law, **Raakel Häggman** and **Åke Häggman**, and to my sister- and brother-in-law, **Ann-Marie Häggman** and **Leif Häggman**, for being my extended family with all the hospitality and love you always give me.

To my grandparents **Hördis Forsberg** and **Nils Hamrin**, for all the support, love and encouragements you gave me during my younger years when you were still here.

To my parents **Britt Mari Forsberg** and **Kent Forsberg**, for giving me all the love and support throughout my life, but unfortunately never got to see this final thesis. I wouldn't be where I am today without you.

To my brother **Leif Forsberg**, and to his partner **Ulrika Öberg**, for all the love and care, and for being there when I need you. I wish you the best in creating your new home in Lomma and I hope to visit you soon.

Above all, I wish to thank my wife **Annika Forsberg** and our two lovely sons, **Lucas Forsberg** and **Anton Forsberg**, for being my family with all the love and care you give me in life. You fill my days with joy.

References

Amunts, K., Mohlberg, H., Bludau, S., and Zilles, K. (2020). Julich-Brain: A 3D probabilistic atlas of the human brain's cytoarchitecture. *Science*, 369(6506):988–992.

Arsalidou, M., Duerden, E. G., and Taylor, M. J. (2013). The centre of the brain: topographical model of motor, cognitive, affective, and somatosensory functions of the basal ganglia. *Human brain mapping*, 34(11):3031 – 3054.

Bajcsy, R., Lieberson, R., and Reivich, M. (1983). A Computerized System for the Elastic Matching of Deformed Radiographic Images to Idealized Atlas Images. *Journal of Computer Assisted Tomography*, 7(4):618–625.

Barrett, R. D. H. and Schluter, D. (2008). Adaptation from standing genetic variation. *Trends in ecology & evolution*, 23(1):38 – 44.

Beckmann, C. F., DeLuca, M., Devlin, J. T., and Smith, S. M. (2005). Investigations into resting-state connectivity using independent component analysis. *Philosophical Transactions of the Royal Society B: Biological Sciences*, 360(1457):1001 – 1013.

Bell, P. T. and Shine, J. M. (2016). Subcortical contributions to large-scale network communication. *Neuroscience and biobehavioral reviews*, 71:313 – 322.

Biswal, B., Yetkin, F. Z., Haughton, V. M., and Hyde, J. S. (1995). Functional connectivity in the motor cortex of resting human brain using echo-planar mri. *Magnetic Resonance in Medicine*, 34(4):537–541.

Blinkouskaya, Y. and Weickenmeier, J. (2021). Brain Shape Changes Associated With Cerebral Atrophy in Healthy Aging and Alzheimer's Disease. *Frontiers in Mechanical Engineering*, 7:705653.

Bohm, C., Greitz, T., Kingsley, D., Berggren, B. M., and Olsson, L. (1983). Adjustable computerized stereotaxic brain atlas for transmission and emission tomography. *AJNR. American journal of neuroradiology*, 4(3):731–3.

Bohm, C., Greitz, T., Seitz, R., and Eriksson, L. (1991). Specification and Selection of Regions of Interest (ROIs) in a Computerized Brain Atlas. *Journal of Cerebral Blood Flow & Metabolism*, 11(1_suppl):A64–A68.

Brett, M., Johnsrude, I. S., and Owen, A. M. (2002). The problem of functional localization in the human brain. *Nature Reviews Neuroscience*, 3(3):243–249.

Brodmann, K. (1909). *Vergleichende Lokalisationslehre der Großhirnrinde in ihren Prinzipien dargestellt auf Grund des Zellenbaues*. Barth, Leipzig.

Bryant, C., Giovanello, K. S., Ibrahim, J. G., Chang, J., Shen, D., Peterson, B. S., Zhu, H., and Initiative, A. D. N. (2013). Mapping the genetic variation of regional brain volumes as explained by all common SNPs from the ADNI study. *PloS one*, 8(8):e71723.

Buckner, R. L., Sepulcre, J., Talukdar, T., Krienen, F. M., Liu, H., Hedden, T., Andrews-Hanna, J. R., Sperling, R. A., and Johnson, K. A. (2009). Cortical hubs revealed by intrinsic functional connectivity: mapping, assessment of stability, and relation to Alzheimer's disease. *The Journal of neuroscience : the official journal of the Society for Neuroscience*, 29(6):1860 – 1873.

Castro, E., Hjelm, R. D., Plis, S. M., Dinh, L., Turner, J. A., and Calhoun, V. D. (2016). Deep Independence Network Analysis of Structural Brain Imaging: Application to Schizophrenia. *IEEE Transactions on Medical Imaging*, 35(7):1729–1740.

Chambers, H. R., Heldstab, S. A., and O'Hara, S. J. (2021). Why big brains? A comparison of models for both primate and carnivore brain size evolution. *PLoS ONE*, 16(12):e0261185.

Charvet, C. J., Darlington, R. B., and Finlay, B. L. (2013). Variation in Human Brains May Facilitate Evolutionary Change toward a Limited Range of Phenotypes. *Brain, Behavior and Evolution*, 81(2):74–85.

Chen, Z. J., He, Y., Rosa-Neto, P., Germann, J., and Evans, A. C. (2008). Revealing Modular Architecture of Human Brain Structural Networks by Using Cortical Thickness from MRI. *Cerebral cortex (New York, N.Y. : 1991)*, 18(10):2374 – 2381.

Cole, M. W., Pathak, S., and Schneider, W. (2010). Identifying the brain's most globally connected regions. *NeuroImage*, 49(4):3132 – 3148.

Collins, D. L. and Evans, A. C. (1997). Animal: Validation and Applications of Nonlinear Registration-Based Segmentation. *International Journal of Pattern Recognition and Artificial Intelligence*, 11(08):1271–1294.

Collins, D. L., Zijdenbos, A. P., Baaré, W. F. C., and Evans, A. C. (1999). Information Processing in Medical Imaging. *Lecture Notes in Computer Science*, pages 210–223.

Dadar, M., Camicioli, R., and Duchesne, S. (2022). Multi sequence average templates for aging and neurodegenerative disease populations. *Scientific Data*, 9(1):238.

DuPre, E. and Spreng, R. N. (2017). Structural covariance networks across the life span, from 6 to 94 years of age. *Network neuroscience (Cambridge, Mass.)*, 1(3):302 – 323.

Eickhoff, S. B., Stephan, K. E., Mohlberg, H., Grefkes, C., Fink, G. R., Amunts, K., and Zilles, K. (2005). A new SPM toolbox for combining probabilistic cytoarchitectonic maps and functional imaging data. *NeuroImage*, 25(4):1325–1335.

Elvsåshagen, T., Shadrin, A., Frei, O., Meer, D. v. d., Bahrami, S., Kumar, V. J., Smeland, O., Westlye, L. T., Andreassen, O. A., and Kaufmann, T. (2021). The genetic architecture of the human thalamus and its overlap with ten common brain disorders. *Nature Communications*, 12(1):2909.

Evans, A., Collins, D., Mills, S., Brown, E., Kelly, R., and Peters, T. (1993). 3D statistical neuroanatomical models from 305 MRI volumes. *1993 IEEE Conference Record Nuclear Science Symposium and Medical Imaging Conference*, pages 1813–1817 vol.3.

Evans, A. C. (2013). Networks of anatomical covariance. *NeuroImage*, 80(C):489 – 504. The review paper on covariance by Evans.

Evans, A. C., Marrett, S., Neelin, P., Collins, L., Worsley, K., Dai, W., Milot, S., Meyer, E., and Bub, D. (1992). Anatomical mapping of functional activation in stereotactic coordinate space. *NeuroImage*, 1(1):43 – 53.

Eyler, L. T., Prom-Wormley, E., Fennema-Notestine, C., Panizzon, M. S., Neale, M. C., Jernigan, T. L., Fischl, B., Franz, C. E., Lyons, M. J., Stevens, A., Pacheco, J., Perry, M. E., Schmitt, J. E., Spitzer, N. C., Seidman, L. J., Thermenos, H. W., Tsuang, M. T., Dale, A. M., and Kremen, W. S. (2011). Genetic patterns of correlation among subcortical volumes in humans: results from a magnetic resonance imaging twin study. *Human brain mapping*, 32(4):641 – 653.

Fillmore, P. T., Phillips-Meek, M. C., and Richards, J. E. (2015). Age-specific MRI brain and head templates for healthy adults from 20 through 89 years of age. *Frontiers in Aging Neuroscience*, 7:44.

Fonov, V., Evans, A., McKinstry, R., Almli, C., and Collins, D. (2009). Unbiased nonlinear average age-appropriate brain templates from birth to adulthood. *NeuroImage*, 47:S102.

Fox, D. (2016). What sparked the Cambrian explosion? *Nature*, 530(7590):268 – 270.

Fox, M. D., Snyder, A. Z., Vincent, J. L., Corbetta, M., Essen, D. C. V., and Raichle, M. E. (2005). The human brain is intrinsically organized into dynamic, anticorrelated functional networks. *Proceedings of the National Academy of Sciences*, 102(27):9673–9678.

Fox, P. T., Perlmutter, J. S., and Raichle, M. E. (1985). A stereotactic method of anatomical localization for positron emission tomography. *Journal of computer assisted tomography*, 9(1):141 – 153.

Fransson, P. (2005). Spontaneous low-frequency BOLD signal fluctuations: an fMRI investigation of the resting-state default mode of brain function hypothesis. *Human brain mapping*, 26(1):15 – 29.

Fransson, P., Skiöld, B., Horsch, S., Nordell, A., Blennow, M., Lagercrantz, H., and Åden, U. (2007). Resting-state networks in the infant brain. *Proceedings of the National Academy of Sciences*, 104(39):15531–15536.

Friedman, L., Kenny, J. T., Wise, A. L., Wu, D., Stuve, T. A., Miller, D. A., Jesberger, J. A., and Lewin, J. S. (1998). Brain Activation During Silent Word Generation Evaluated with Functional MRI. *Brain and Language*, 64(2):231–256.

Friston, K. J., Frith, C. D., Liddle, P. F., and Frackowiak, R. S. (1993). Functional connectivity: the principal-component analysis of large (PET) data sets. *Journal of cerebral blood flow and metabolism : official journal of the International Society of Cerebral Blood Flow and Metabolism*, 13(1):5 – 14.

Friston, K. J., Josephs, O., Rees, G., and Turner, R. (1998). Nonlinear event-related responses in fMRI. *Magnetic Resonance in Medicine*, 39(1):41–52.

Glover, G. H. (2011). Overview of Functional Magnetic Resonance Imaging. *Neurosurgery Clinics of North America*, 22(2):133–139.

Good, C. D., Johnsrude, I. S., Ashburner, J., Henson, R. N., Friston, K. J., and Frackowiak, R. S. (2001). A voxel-based morphometric study of ageing in 465 normal adult human brains. *NeuroImage*, 14(1 Pt 1):21 – 36.

Grabner, G., Janke, A. L., Budge, M. M., Smith, D., Pruessner, J., and Collins, D. L. (2006). Symmetric atlasing and model based segmentation: an application to the hippocampus in older adults. *Medical image computing and computer-assisted intervention : MICCAI ... International Conference on Medical Image Computing and Computer-Assisted Intervention*, 9(Pt 2):58 – 66.

Greicius, M. D., Krasnow, B., Reiss, A. L., and Menon, V. (2003). Functional connectivity in the resting brain: A network analysis of the default mode hypothesis. *Proceedings of the National Academy of Sciences*, 100(1):253–258.

Grillner, S. and Robertson, B. (2016). The Basal Ganglia Over 500 Million Years. *Current biology : CB*, 26(20):R1088 – R1100.

Hanson, A., Grisham, W., Sheh, C., Annese, J., and Ridgway, S. (2013). Quantitative Examination of the Bottlenose Dolphin Cerebellum. *The Anatomical Record*, 296(8):1215–1228.

Harris, T. B., Launer, L., Eiriksdottir, G., Kjartansson, O., Jonsson, P. V., Sigurdsson, G., Thorgeirsson, G., Aspelund, T., Garcia, M. E., Cotch, M. F., Hoffman, H. J., and Gudnason, V. (2007). Age, Gene/Environment Susceptibility-Reykjavik Study: multidisciplinary applied phenomics. *American journal of epidemiology*, 165(9):1076 – 1087.

He, Y., Chen, Z. J., and Evans, A. C. (2007). Small-world anatomical networks in the human brain revealed by cortical thickness from MRI. *Cerebral cortex (New York, N.Y. : 1991)*, 17(10):2407 – 2419.

Herscovitch, P., Markham, J., and Raichle, M. E. (1983). Brain blood flow measured with intravenous H2(15)O. I. Theory and error analysis. *Journal of nuclear medicine : official publication, Society of Nuclear Medicine*, 24(9):782–9.

Holmes, C. J., Hoge, R., Louis, C., Woods, R., Toga, A. W., and Evans, A. C. (1998). Enhancement of MR Images Using Registration for Signal Averaging. *Journal of Computer Assisted Tomography*, 22(2):324–333.

Idelberger, K. (1936). Die Verdienste Friedrich Tiedemanns um die Anatomie des Gehirns. *Archiv für Psychiatrie und Nervenkrankheiten*, 105(1):250–290.

Ingvar, D. H. and Risberg, J. (1967). Increase of regional cerebral blood flow during mental effort in normals and in patients with focal brain disorders. *Experimental Brain Research*, 3(3):195–211.

Kaiser, M. and Varier, S. (2011). Evolution and development of Brain Networks: From Caenorhabditis elegans to Homo sapiens. *Network: Computation in Neural Systems*, 22(1-4):143–147.

Kety, S. S. and Schmidt, C. F. (1945). The Determination of Cerebral Blood Flow in Man by the Use of Nitrous Oxide in Low Concentrations. *American Journal of Physiology-Legacy Content*, 143(1):53–66.

Kingma, D. P. and Welling, M. (2013). Auto-Encoding Variational Bayes. *arxiv.org*.

Klein, A., Andersson, J., Ardekani, B. A., Ashburner, J., Avants, B., Chiang, M.-C., Christensen, G. E., Collins, D. L., Gee, J., Hellier, P., Song, J. H., Jenkinson, M., Lepage, C., Rueckert, D., Thompson, P., Vercauteren, T., Woods, R. P., Mann, J. J., and Parsey, R. V. (2009). Evaluation of 14 nonlinear deformation algorithms applied to human brain MRI registration. *NeuroImage*, 46(3):786–802.

Lai, Y.-T., Yeung, C. K. L., Omland, K. E., Pang, E.-L., Hao, Y., Liao, B.-Y., Cao, H.-F., Zhang, B.-W., Yeh, C.-F., Hung, C.-M., Hung, H.-Y., Yang, M.-Y., Liang, W., Hsu, Y.-C., Yao, C.-T., Dong, L., Lin, K., and Li, S.-H. (2019). Standing genetic variation as the predominant source for adaptation of a songbird. *Proceedings of the National Academy of Sciences of the United States of America*, 116(6):2152 – 2157.

Lancaster, J. L., Rainey, L. H., Summerlin, J. L., Freitas, C. S., Fox, P. T., Evans, A. C., Toga, A. W., and Mazziotta, J. C. (1997). Automated labeling of the human brain: a preliminary report on the development and evaluation of a forward-transform method. *Human brain mapping*, 5(4):238–42.

Lancaster, J. L., Tordesillas-Gutiérrez, D., Martinez, M., Salinas, F., Evans, A., Zilles, K., Mazziotta, J. C., and Fox, P. T. (2007). Bias between MNI and Talairach coordinates analyzed using the ICBM-152 brain template. *Human brain mapping*, 28(11):1194 – 1205.

LaPointe, L. L. (2014). Paul Broca and French Brains. *Communication Disorders Quarterly*, 36(1):29–34.

Lassen, N. A. and Ingvar, D. H. (1961). The blood flow of the cerebral cortex determined by radioactive krypton. *Experientia*, 17:42–3.

Mace, G. M., Harvey, P. H., and Clutton-Brock, T. H. (1981). Brain size and ecology in small mammals. *Journal of Zoology*, 193(3):333–354.

Macmillan, M. (2005). Localization and William Macewen's Early Brain Surgery Part II: The Cases. *Journal of the History of the Neurosciences*, 14(1):24–56.

Manzano, O. d. and Ullén, F. (2018). Same Genes, Different Brains: Neuroanatomical Differences Between Monozygotic Twins Discordant for Musical Training | Cerebral Cortex | Oxford Academic. *academic.oup.com*.

Martinez-Murcia, F. J., Ortiz, A., Gorriz, J.-M., Ramirez, J., and Castillo-Barnes, D. (2020). Studying the Manifold Structure of Alzheimer's Disease: A Deep Learning Approach Using Convolutional Autoencoders. *IEEE journal of biomedical and health informatics*, 24(1):17 – 26.

Martino, A. D., Yan, C.-G., Li, Q., Denio, E., Castellanos, F. X., Alaerts, K., Anderson, J. S., Assaf, M., Bookheimer, S. Y., Dapretto, M., Deen, B., Delmonte, S., Dinstein, I., Ertl-Wagner, B., Fair, D. A., Gallagher, L., Kennedy, D. P., Keown, C. L., Keysers, C., Lainhart, J. E., Lord, C., Luna, B., Menon, V., Minshew, N. J., Monk, C. S., Mueller, S., Müller, R.-A., Nebel, M. B., Nigg, J. T., O'Hearn, K., Pelphrey, K. A., Peltier, S. J., Rudie, J. D., Sunaert, S., Thioux, M., Tyszka, J. M., Uddin, L. Q., Verhoeven, J. S., Wenderoth, N., Wiggins, J. L., Mostofsky, S. H., and Milham, M. P. (2014). The autism brain imaging data exchange: towards a large-scale evaluation of the intrinsic brain architecture in autism. *Molecular psychiatry*, 19(6):659 – 667.

Mazoyer, B. (2008). *In memoriam: Jean Talairach (1911-2007): a life in stereotaxy.*, volume 29 of *Human brain mapping*. Hum Brain Mapp.

Mazziotta, J., Toga, A., Evans, A., Fox, P., Lancaster, J., Zilles, K., Woods, R., Paus, T., Simpson, G., Pike, B., Holmes, C., Collins, L., Thompson, P., MacDonald, D., Iacoboni, M., Schormann, T., Amunts, K., Palomero-Gallagher, N., Geyer, S., Parsons, L., Narr, K., Kabani, N., Goualher, G. L., Boomsma, D., Cannon, T., Kawashima, R., and Mazoyer, B. (2001a). A probabilistic atlas and reference system for the human brain: International Consortium for Brain Mapping (ICBM). *Philosophical transactions of the Royal Society of London. Series B, Biological sciences*, 356(1412):1293 – 1322.

Mazziotta, J., Toga, A., Evans, A., Fox, P., Lancaster, J., Zilles, K., Woods, R., Paus, T., Simpson, G., Pike, B., Holmes, C., Collins, L., Thompson, P., MacDonald, D., Iacoboni, M., Schormann, T., Amunts, K., Palomero-Gallagher, N., Geyer, S., Parsons, L., Narr, K., Kabani, N., Goualher, G. L., Feidler, J., Smith, K., Boomsma, D., Pol, H. H., Cannon, T., Kawashima, R., and Mazoyer, B. (2001b). A Four-Dimensional Probabilistic Atlas of the Human Brain. *Journal of the American Medical Informatics Association*, 8(5):401–430.

Mechelli, A., Friston, K. J., Frackowiak, R. S., and Price, C. J. (2005). Structural covariance in the human cortex. *The Journal of neuroscience : the official journal of the Society for Neuroscience*, 25(36):8303 – 8310. Main reference for structural covariance (2006).

Morgane, P. J., Glezer, I. I., and Jacobs, M. S. (1990). Cerebral Cortex - Comparative and Evolutionary Anatomy of the Visual Cortex of the Dolphin. *Cerebral Cortex*, pages 215–262.

Ogawa, S., Lee, T. M., Kay, A. R., and Tank, D. W. (1990). Brain magnetic resonance imaging with contrast dependent on blood oxygenation. *Proceedings of the National Academy of Sciences*, 87(24):9868–9872.

Parent, A. and Hazrati, L.-N. (1995). Functional anatomy of the basal ganglia. I. The cortico-basal ganglia-thalamo-cortical loop. *Brain Research Reviews*, 20(1):91–127.

Pillmann, F. (2003). Carl Wernicke (1848–1905). *Journal of Neurology*, 250(11):1390–1391.

Raichle, M. E., MacLeod, A. M., Snyder, A. Z., Powers, W. J., Gusnard, D. A., and Shulman, G. L. (2001). A default mode of brain function. *Proceedings of the National Academy of Sciences*, 98(2):676–682.

Raichle, M. E., Martin, W. R., Herscovitch, P., Mintun, M. A., and Markham, J. (1983). Brain blood flow measured with intravenous H2(15)O. II. Implementation and validation. *Journal of nuclear medicine : official publication, Society of Nuclear Medicine*, 24(9):790–8.

Reid, A. T., Hoffstaedter, F., Gong, G., Laird, A. R., Fox, P., Evans, A. C., Amunts, K., and Eickhoff, S. B. (2017). A seed-based cross-modal comparison of brain connectivity measures. *Brain structure & function*, 222(3):1131 – 1151.

Risberg, J. and Ingvar, D. H. (1973). Patterns of activation in the grey matter of the dominant hemisphere during memorizing and reasoning. A study of regional cerebral blood flow changes during psychological testing in a group of neurologically normal patients. *Brain*, 96(4):737–756.

Roland, P. E., Graufelds, C. J., Hlin, J. W., Ingelman, L., Andersson, M., Ledberg, A., Pedersen, J., Akerman, S., Dabringhaus, A., and Zilles, K. (1994). Human brain atlas: For high-resolution functional and anatomical mapping. *Human brain mapping*, 1(3):173 – 184.

Roland, P. E. and Larsen, B. (1976). Focal Increase of Cerebral Blood Flow During Stereognostic Testing in Man. *Archives of Neurology*, 33(8):551–558.

Roland, P. E., Larsen, B., Lassen, N. A., and Skinhoj, E. (1980). Supplementary motor area and other cortical areas in organization of voluntary movements in man. *Journal of Neurophysiology*, 43(1):118–136.

Roy, C. S. and Sherrington, C. S. (1890). On the Regulation of the Blood-supply of the Brain. *The Journal of Physiology*, 11(1-2):85–158.

Rubinov, M. and Sporns, O. (2010). Complex network measures of brain connectivity: Uses and interpretations. *NeuroImage*, 52(3):1059 – 1069.

Sandrone, S., Bacigaluppi, M., Galloni, M. R., Cappa, S. F., Moro, A., Catani, M., Filippi, M., Monti, M. M., Perani, D., and Martino, G. (2014). Weighing brain activity with the balance: Angelo Mosso's original manuscripts come to light. *Brain*, 137(2):621–633.

Segall, J. M., Allen, E. A., Jung, R. E., Erhardt, E. B., Arja, S. K., Kiehl, K., and Calhoun, V. D. (2012). Correspondence between structure and function in the human brain at rest. *Frontiers in Neuroinformatics*, 6:10.

Sigurdsson, S., Aspelund, T., Forsberg, L., Fredriksson, J., Kjartansson, O., Oskarsdottir, B., Jonsson, P. V., Eiriksdottir, G., Harris, T. B., Zijdenbos, A., Buchem, M. A. v., Launer, L., and Gudnason, V. (2012). Brain tissue volumes in the general population of the elderly: the AGES-Reykjavik study. *NeuroImage*, 59(4):3862 – 3870.

Smith, S., Duff, E., Groves, A., Nichols, T. E., Jbabdi, S., Westlye, L. T., Tamnes, C. K., Engvig, A., Walhovd, K. B., Fjell, A. M., Johansen-Berg, H., and Douaud, G. (2019). Structural Variability in the Human Brain Reflects Fine-Grained Functional Architecture at the Population Level. *The Journal of neuroscience : the official journal of the Society for Neuroscience*, 39(31):6136 – 6149.

Smith, S. M., Fox, P. T., Miller, K. L., Glahn, D. C., Fox, P. M., Mackay, C. E., Filippini, N., Watkins, K. E., Toro, R., Laird, A. R., and Beckmann, C. F. (2009). Correspondence of the brain's functional architecture during activation and rest. *Proceedings of the National Academy of Sciences of the United States of America*, 106(31):13040 – 13045.

Smith, S. M., Jenkinson, M., Woolrich, M. W., Beckmann, C. F., Behrens, T. E. J., Johansen-Berg, H., Bannister, P. R., Luca, M. D., Drobnjak, I., Flitney, D. E., Niazy, R. K., Saunders, J., Vickers, J., Zhang, Y., Stefano, N. D., Brady, J. M., and Matthews, P. M. (2004). Advances in functional and structural MR image analysis and implementation as FSL. *NeuroImage*, 23 Suppl 1:S208 – 19.

Soriano-Mas, C., Harrison, B. J., Pujol, J., López-Solà, M., Hernández-Ribas, R., Alonso, P., Contreras-Rodríguez, O., Giménez, M., Blanco-Hinojo, L., Ortiz, H., Deus, J., Menchón, J. M., and Cardoner, N. (2013). Structural covariance of the neostriatum with regional gray matter volumes. *Brain structure & function*, 218(3):697 – 709.

Stephenson-Jones, M., Samuelsson, E., Ericsson, J., Robertson, B., and Grillner, S. (2011). Evolutionary conservation of the basal ganglia as a common vertebrate mechanism for action selection. *Current biology : CB*, 21(13):1081 – 1091.

Strotzer, M. (2009). One century of brain mapping using Brodmann areas. *Klinische Neuroradiologie*, 19(3):179–86.

Talairach, J. and Tournoux, P. (1988). *Co-planar Stereotaxic Atlas of the Human Brain: 3-dimensional Proportional System : an Approach to Cerebral Imaging*. Thieme. Thieme.

Triarhou, L. C. (2021). Pre-Brodmann pioneers of cortical cytoarchitectonics I: Theodor Meynert, Vladimir Betz and William Bevan-Lewis. *Brain Structure and Function*, 226(1):49–67.

Tzourio-Mazoyer, N., Landeau, B., Papathanassiou, D., Crivello, F., Etard, O., Delcroix, N., Mazoyer, B., and Joliot, M. (2002). Automated anatomical labeling of activations in SPM using a macroscopic anatomical parcellation of the MNI MRI single-subject brain. *NeuroImage*, 15(1):273 – 289.

Wickens, J. R. (2009). Synaptic plasticity in the basal ganglia. *Behavioural brain research*, 199(1):119 – 128.

Wright, I. C., McGuire, P. K., Poline, J. B., Travere, J. M., Murray, R. M., Frith, C. D., Frackowiak, R. S., and Friston, K. J. (1995). A voxel-based method for the statistical analysis of gray and white matter density applied to schizophrenia. *NeuroImage*, 2(4):244 – 252.

Wu, K., Taki, Y., Sato, K., Kinomura, S., Goto, R., Okada, K., Kawashima, R., He, Y., Evans, A. C., and Fukuda, H. (2012). Age-related changes in topological organization of structural brain networks in healthy individuals. *Human brain mapping*, 33(3):552 – 568.

Xu, L., Groth, K. M., Pearlson, G., Schretlen, D. J., and Calhoun, V. D. (2009). Source-based morphometry: the use of independent component analysis to identify gray matter differences with application to schizophrenia. *Human brain mapping*, 30(3):711 – 724.

Zhang, Z., Liao, W., Zuo, X.-N., Wang, Z., Yuan, C., Jiao, Q., Chen, H., Biswal, B. B., Lu, G., and Liu, Y. (2011). Resting-state brain organization revealed by functional covariance networks. *PloS one*, 6(12):e28817.

Zhao, B., Ibrahim, J. G., Li, Y., Li, T., Wang, Y., Shan, Y., Zhu, Z., Zhou, F., Zhang, J., Huang, C., Liao, H., Yang, L., Thompson, P. M., and Zhu, H. (2019). Heritability of Regional Brain Volumes in Large-Scale Neuroimaging and Genetic Studies. *Cerebral cortex (New York, N.Y. : 1991)*, 29(7):2904 – 2914.

Zijdenbos, A. P., Forghani, R., and Evans, A. C. (2002). Automatic "pipeline" analysis of 3-D MRI data for clinical trials: application to multiple sclerosis. *IEEE transactions on medical imaging*, 21(10):1280 – 1291.

Zilles, K. (2018). Brodmann: a pioneer of human brain mapping—his impact on concepts of cortical organization. *Brain*, 141(11):3262–3278.